DMD Fast Forward. Published on November 8, 2017 as DOI: 10.1124/dmd.117.078006
This article has not been copyedited and formatted. The final version may differ from this version.

DMD # 078006

Simultaneous physiologically based pharmacokinetic (PBPK) modeling of parent and active metabolites to investigate complex CYP3A4 drug-drug interaction potential: a case example of midostaurin

Helen Gu, Catherine Dutreix, Sam Rebello, Taoufik Ouatas, Lai Wang, Dung Yu Chun, Heidi J. Einolf, Handan He

Primary affiliations of all authors: HG, SR, LW, DYC, HJE, and HH: Novartis Pharmaceuticals Corporation, East Hanover, New Jersey, USA. CD and TO: Basel, Switzerland. DYC: Insmed Inc., Bridgewater, New Jersey, USA.

Laboratory of origin: same as affiliations

DMD Fast Forward. Published on November 8, 2017 as DOI: 10.1124/dmd.117.078006
This article has not been copyedited and formatted. The final version may differ from this version.

RUNNING TITLE PAGE

Running title: PBPK modeling for midostaurin-CYP3A4 interaction

Corresponding author: Helen Gu, Novartis Pharmaceuticals Corporation, One Health Plaza, East Hanover, NJ 07936

telephone: 1-862-778-5722

fax: 1-973-781-7579

e-mail: helen.gu@novartis.com

Text pages:	23
Tables:	5
Figures:	7
References:	38

Word count:

Abstract:	249
Introduction:	748
Discussion:	1500

DMD Fast Forward. Published on November 8, 2017 as DOI: 10.1124/dmd.117.078006
This article has not been copyedited and formatted. The final version may differ from this version.

Abbreviations

4βHC, 4β-hydroxycholesterol
ADME, absorption, distribution, metabolism, and excretion
advSM, advanced systemic mastocytosis
AGP, α1-acid glycoprotein
AML, acute myeloid leukemia
AUC, area under the curve
bid, twice daily
B/P, blood-to-plasma ratio
Caco-2, continuous heterogeneous human epithelial colorectal adenocarcinoma cell line
CL, clearance
CL/F, apparent oral clearance
CL_{int}, intrinsic clearance
CL_R, renal clearance
C_{max}, maximum concentration
CYP, cytochrome P450
CYP3A4, cytochrome P450 3A4
DDI, drug-drug interaction
EC_{50}, concentration of inducer at half E_{max}
E_{max}, maximal induction
F_a, fraction of dose absorbed
F_g, fraction of the dose that escapes presystemic intestinal first-pass elimination
FLT3, fms-like tyrosine kinase 3
fm_{CYP3A4}, fraction metabolized by CYP3A4
$fm_{CGP52421}$, fractions of total CGP52421 metabolism catalyzed by CYP3A4
$fm_{CGP62221}$, fractions of total CGP62221 metabolism catalyzed by CYP3A4
$fm_{other\ 3A4}$, fractions of total other metabolite metabolism catalyzed by CYP3A4
FMI, final market image
fu_{gut}, fraction of unbound drug in the gut
fu_{mic}, fraction of unbound drug in microsomes
fu_p, fraction of unbound drug in plasma
GM, geometric mean
GMR, geometric mean ratio
HLM, human liver microsome
Ind_{50}, half-maximum induction rate
Ind_{max}, maximum induction rate
inf, infinity
ITD, internal tandem duplication
k_a, absorption rate constant
K_I, concentration producing a half-maximal rate of activity reduction
k_{in}, zero-order rate constant for the formation of a physiological response variable
k_{inact}, maximal rate of activity reduction
K_{iu}, unbound inhibition constant
k_{out}, first-order rate constant for the degradation of a physiological response variable
LC-MS/MS, liquid chromatography–tandem mass spectrometry
logPo:w, water partition coefficient
MW, molecular weight

DMD Fast Forward. Published on November 8, 2017 as DOI: 10.1124/dmd.117.078006
This article has not been copyedited and formatted. The final version may differ from this version.

NA, not applicable
PBPK, physiologically based pharmacokinetic
Peff, man, effective permeability in man
PK, pharmacokinetics
pKa, acid dissociation constant
Pop PK, population pharmaceutics
Q, intercompartmental clearance
qd, once daily
Q_{gut}, nominal flow through the gut
SM, systemic mastocytosis
TDI, time-dependent inhibitor
TKD, tyrosine kinase domain
t_{lag}, lag time
T_{max}, time at which C_{max} is reached
V_{sac}, volume of distribution for the single adjustable compartment
V_{ss}, volume of distribution at steady state
V_z/F, apparent volume of distribution

DMD Fast Forward. Published on November 8, 2017 as DOI: 10.1124/dmd.117.078006
This article has not been copyedited and formatted. The final version may differ from this version.

ABSTRACT

Midostaurin (PKC412) is being investigated for the treatment of acute myeloid leukemia (AML) and advanced systemic mastocytosis (advSM). It is extensively metabolized by cytochrome P450 (CYP) 3A4 to form 2 major active metabolites, CGP52421 and CGP62221. In vitro and clinical drug-drug interaction (DDI) studies indicated that midostaurin and its metabolites are substrates, reversible and time-dependent inhibitors, and inducers of CYP3A4. A simultaneous pharmacokinetic model of parent and active metabolites was initially developed by incorporating data from in vitro, preclinical, and clinical pharmacokinetic studies in healthy volunteers and in patients with AML or advSM. The model reasonably predicted changes in midostaurin exposure after single-dose administration with ketoconazole (5.8-fold predicted vs 6.1-fold observed increase) and rifampicin (90% predicted vs 94% observed reduction) as well as changes in midazolam exposure (1.0 predicted vs 1.2 observed ratio) after daily dosing of midostaurin for 4 days. The qualified model was then applied to predict the DDI effect with other CYP3A4 inhibitors or inducers and DDI potential with midazolam under steady-state conditions. The simulated midazolam AUC ratio of 0.54 and accompanying observed 1.9-fold increase in the CYP3A4 activity biomarker 4β-hydroxycholesterol indicated a weak-to-moderate CYP3A4 induction by midostaurin and its metabolites at steady state in patients with advSM. In conclusion, a simultaneous parent-and-active-metabolite modeling approach allowed predictions under steady-state conditions that were not possible to achieve in healthy subjects. Furthermore, endogenous biomarker data enabled evaluation of the net effect of midostaurin and its metabolites on CYP3A4 activity at steady state and increased confidence in DDI predictions.

DMD Fast Forward. Published on November 8, 2017 as DOI: 10.1124/dmd.117.078006
This article has not been copyedited and formatted. The final version may differ from this version.

INTRODUCTION

Midostaurin is a potent kinase inhibitor of fms-like tyrosine kinase 3 (FLT3), KIT (including D816V and Y mutants), platelet-derived growth factor receptor beta, vascular endothelial growth factor receptor 2, fibroblast growth factor receptor, and protein kinase C. FLT3 mutations occur in approximately 30% of patients with acute myeloid leukemia (AML). Midostaurin is equally active against FLT3 with internal tandem duplications (ITDs) and with tyrosine kinase domain (TKD) mutations and has been shown to inhibit other kinases implicated in diseases, including KIT in advanced systemic mastocytosis (advSM) (Gotlib et al., 2005; Weisberg et al., 2002; Barry et al., 2007; Andrejauskas-Buchdunger and Regenass, 1992; Fabbro et al., 2000; Stone et al., 2005; Propper et al., 2001). Midostaurin is in clinical development for *FLT3*-mutated AML and advSM (Stone et al., 2005; Gallogly and Lazarus, 2016; Gotlib et al., 2016; Fischer et al., 2010). Based primarily on the phase 3 RATIFY clinical study (Stone et al., 2015), the US Food and Drug Administration (FDA) granted approval to midostaurin in April 2017.

Midostaurin is rapidly and almost completely absorbed in humans after oral administration (Yin et al, 2008; Dutreix et al, 2013) and is highly distributed. Midostaurin is extensively metabolized by cytochrome P450 (CYP) 3A4 to form its 2 metabolites, CGP52421 (7-hydroxylation, epimer 2) and CGP62221 (*O*-demethylation) (Yin et al., 2008; Wang et al., 2008). Elimination is primarily through fecal excretion, mostly as metabolites. CGP52421 and CGP62221 have also been identified as being pharmacologically active against cells expressing *FLT3*-ITDs and *KIT* D816V (Propper et al., 2001). Midostaurin (concentration of inducer at half maximal induction of cytotoxicity response [EC_{50}] 39 and 47 nM for *FLT3*-ITDs and *KIT* D816V, respectively) and CGP62221 (EC_{50} 30 and 70 nM for *FLT3*-ITDs and *KIT* D816V,

DMD Fast Forward. Published on November 8, 2017 as DOI: 10.1124/dmd.117.078006
This article has not been copyedited and formatted. The final version may differ from this version.

respectively) showed similar potency (Levis et al., 2006), whereas CGP52421 showed approximately average 10-fold reduced potency (EC_{50} 656 and 233 nM for *FLT3*-ITDs and *KIT* D816V, respectively). Both metabolites were also found to be CYP3A4 substrates (Dutreix et al. 2013). Therefore, drug-drug interactions (DDIs) can result in exposure alterations of midostaurin and its metabolites when co-administered with drugs that inhibit or induce CYP3A4. Furthermore, midostaurin and its 2 active metabolites were reversible and time-dependent inhibitors and inducers of CYP3A4 in vitro. These mixed CYP3A4 interactions can potentially affect the exposure of victim drugs when co-administered with drugs that are sensitive CYP3A4 substrates (eg, midazolam). Due to these complex DDI mechanisms, midostaurin and its metabolites can act as CYP3A4 substrates, inhibitors, and inducers and also affect their own metabolic clearance (FDA 2012; EMA 2012; Prueksaritanont et al., 2013; Fenneteau et al., 2010; Fahmi et al., 2009; Garg et al., 2012; Yeo et al., 2011; Reitman et al., 2011) or that of other drugs.

In the initial phase of development, DDI studies were conducted in healthy volunteers to address the clinical relevance of CYP3A4-related DDIs, with midostaurin as either a victim of a ketoconazole or rifampicin interaction or a perpetrator of midazolam (Dutreix et al., 2013; Dutreix et al., 2014). However, these early clinical studies were conducted mostly using relatively short dosing periods. The terminal half-lives of midostaurin, CGP62221, and CGP52421 in plasma are 19.6, 32.2, and 482 hours, respectively. Due to the complex DDI mechanisms of midostaurin and its metabolites, it is important to evaluate potential DDIs under steady-state conditions to support clinical recommendations and potential product label language. Because such DDI studies are not feasible in healthy subjects, we aimed to use a multipronged approach to investigate the net effect of steady-state midostaurin on CYP3A4

DMD Fast Forward. Published on November 8, 2017 as DOI: 10.1124/dmd.117.078006
This article has not been copyedited and formatted. The final version may differ from this version.

activity. To achieve this goal, we (1) built a physiologically based pharmacokinetic (PBPK) model to describe the pharmacokinetics (PK) of midostaurin and its 2 active metabolites using a top-down approach leveraging prior clinical PK data in both healthy subjects and patients; (2) verified the model's performance in predicting clinical PK profiles of midostaurin and its metabolites, particularly in simulating clinically observed DDIs under single-dose conditions; and (3) used the model to predict CYP3A4-related DDIs with midostaurin at steady state. Furthermore, the utility of the endogenous plasma biomarker 4β-hydroxycholesterol (4βHC) as a tool for assessing CYP3A4 activity was explored to address the uncertainty in evaluating the net effect of CYP3A4 induction or inhibition of new molecular entities that have mixed inhibition or induction DDI mechanisms in vitro. The final model was also used to predict DDI potential with other CYP3A4 substrates, inhibitors, and inducers; the model limitations are discussed. The prediction results from our case example provide a basis for optimal clinical study recommendations and potential label language.

MATERIALS AND METHODS

PBPK modeling was accomplished following these general steps: (1) the model was initially developed using physiochemical data; absorption, distribution, metabolism, and excretion (ADME) data; and in vitro DDI study data and optimized to fit the clinical PK data of the parent and its 2 metabolites; (2) the model was verified by comparing simulated data with data from clinical DDI studies; and (3) the model was applied to predict potential DDI effects of CYP3A4 inhibitors or inducers on midostaurin and its metabolites as well as effects on midazolam under steady-state conditions. Finally, the results from plasma 4βHC levels (fold

DMD Fast Forward. Published on November 8, 2017 as DOI: 10.1124/dmd.117.078006
This article has not been copyedited and formatted. The final version may differ from this version.

change relative to baseline) were used to confirm the net effect of time-dependent inhibition/induction of CYP3A4 by midostaurin and its metabolites.

PBPK Model Development in Healthy Subjects

A PBPK model was built using Simcyp Simulator, version 15, release 1 (Certara, LP, Princeton, NJ) for midostaurin and its 2 metabolites, CGP52421 and CGP62221, using in vitro ADME and in vivo PK data (Table 1). The key input parameters are described here.

Physiochemical Properties and Plasma Binding

The molecular weights of midostaurin, CGP52421, and CGP62221 are 570.6, 586.6, and 556.6 g/mol, respectively, and the water partition coefficient (logP octanol:water) ratios used were 5.5, 4.8, and 4.7 (calculated logP values), respectively. The compound type was entered as a monoprotic base, with a pKa value of 11.2 for midostaurin and CGP62221 and a pKa value of 10.8 for CGP52421 (predicted using ADMET Predictor 6.5, Simulations Plus, Lancaster, CA). The blood-to-plasma ratios for midostaurin, CGP62221, and CGP52421 were entered as 0.55 based on the internal experimental values.

The fractions bound to plasma for all 3 components were very high (> 99%). For these very highly bound compounds, an equilibrium gel filtration method was used (He et al., 2017; Weiss et al., 2014). Midostaurin was mainly bound to human α1-acid glycoprotein (AGP) according to an internal study. Therefore, AGP was selected as a plasma-binding component in the model.

Absorption

A first-order model for midostaurin absorption from the gut lumen was chosen. Several key input parameters were applied. First, the fraction of dose absorbed (F_a) was entered as 0.85, primarily to optimize maximum concentration (C_{max}), based on the observed data from a single

DMD Fast Forward. Published on November 8, 2017 as DOI: 10.1124/dmd.117.078006
This article has not been copyedited and formatted. The final version may differ from this version.

oral midostaurin 50-mg dose in a prior clinical study. This F_a value was consistent with the moderate to high absorption observed in preclinical species and humans (He et al., 2017). The absorption rate constant and lag time were user defined as 1.5 1/h and 0.3 hours, respectively, to optimize C_{max} and T_{max} that were observed in several clinical trials (after a single dose). Second, the fraction of unbound drug in the gut (fu_{gut}) was predicted to be 0.3, and, accordingly, by Simcyp, the output fraction of the dose that escapes presystemic intestinal first-pass elimination (F_g) value was 0.15, a value derived from the Simcyp-predicted fu_{gut} value. This predicted human F_g was consistent with the observed rat F_g based on calculations from data obtained in a rat in vivo study (data not shown). Finally, the nominal flow through the gut value captures the fact that a higher permeability past the enzyme will decrease first-pass exposure to the enzyme, as will a greater blood flow carrying drug away from the enterocytes. The value was predicted to be 5.23 L/h with Simcyp, using the apparent permeability data from an internal continuous heterogeneous human epithelial colorectal adenocarcinoma cell line (Caco-2) study.

Distribution

The minimal PBPK model in Simcyp was used with a single adjusting compartment for all 3 components. The volume of distribution at steady state (V_{ss}) was estimated to be 1 L/kg, with parameters for a Q (intercompartmental clearance) of 3 L/h and a volume of distribution for the single adjustable compartment (V_{sac}) of 0.82 L/kg. The estimated midostaurin oral V_{ss} was close to the observed geometric mean (GM) or median apparent volume of distribution values, which ranged from 1.0 to 1.3 L/kg. For CGP52421, V_{ss} was estimated to be 1.8 L/kg, with a Q of 10 L/h and a V_{sac} of 1.3 L/kg. For CGP62221, V_{ss} was estimated to be 1.3 L/kg, with a Q of 2 L/h and a V_{sac} of 1.1 L/kg. All values were estimated based on optimization to best fit to PK data from clinical trials (Supplemental Table 9).

DMD Fast Forward. Published on November 8, 2017 as DOI: 10.1124/dmd.117.078006
This article has not been copyedited and formatted. The final version may differ from this version.

Elimination

The retrograde model was used to calculate in vitro intrinsic clearance (CL_{int}) values of the relevant metabolizing enzymes from intravenous or apparent oral clearance (CL/F). In brief, the CL/F of 2.4 L/h was estimated to optimize the plasma concentration-time profiles of midostaurin observed in the clinical trials used for model development. This estimated oral clearance value was consistent with the observed median or GM CL/F values, which ranged from 2.1 to 3.8 L/h. The fraction metabolized by CYP3A4 (fm_{CYP3A}) was set to a value of 1 for midostaurin based on human in vitro findings and the human ADME study. As such, CYP3A4 CL_{int} was calculated to be ≈25.2 µL/min/mg/pmol of CYP3A4 by the retrograde model for enzyme kinetics in Simcyp. In a second step, the CYP3A4 CL_{int} was divided between the involved elimination pathways (ie, CGP52421, CGP62221, and other CYP3A4-mediated pathway[s]). The fraction of CYP3A4 for the metabolism (formation of CGP52421 and CGP62221)/elimination of midostaurin was estimated. The estimations are based mainly on an enzyme phenotyping study using human liver microsomes (HLMs) and CYP-selective chemical inhibitors; the estimations showed that CYP3A4 contributed to most of the hepatic oxidative microsomal metabolism of midostaurin. Furthermore, CGP52421 and CGP62221 are also metabolized mainly by CYP3A4. The human ADME study (He et al., 2017) showed that midostaurin undergoes extensive metabolism and is predominantly excreted through feces, mostly as metabolites. The fractions of CYP3A4 for the metabolism/elimination of midostaurin in human fecal excreta were estimated to be 37%, 37%, and 26% for CGP52421, CGP62221, and other minor metabolites, respectively. Consequently, the values of CL_{int} in µL/min/pmol of CYP3A4 were assigned to the following CYP3A4 pathways: CGP52421, 9.3; CGP62221, 9.3; other CYP3A4, 6.6 (µL/min/pmol of CYP3A4).

DMD Fast Forward. Published on November 8, 2017 as DOI: 10.1124/dmd.117.078006
This article has not been copyedited and formatted. The final version may differ from this version.

For the oral CL/F, the values were estimated to be 0.4 and 0.27 L/h for CGP52421 and CGP62221, respectively, based on optimization to best fit to the plasma concentration-time profiles of these metabolites from clinical trials. Furthermore, it was assumed that approximately 90% of CGP52421 and CGP62221 clearance was mediated by CYP3A4, as they were detected at low levels in human excreta. The CYP3A4 CL_{int} values derived from the CL/F were predicted by the retrograde model to be 3.18 µL/min/pmol of CYP3A4 and 1.19 µL/min/pmol of CYP3A4 for CGP52421 and CGP62221, respectively.

Data from the human ADME study indicated that midostaurin in urine was not detected, as shown in a high-performance liquid chromatography profile of radioactive components in pooled urine (0-72 h). Therefore, the renal CL was assumed to be negligible and set to 0 L/h.

Interaction

The potential of midostaurin, CGP52421, and CGP62221 to inhibit human CYP3A4/5 enzyme activity and act as CYP3A4/5 time-dependent inhibitors (TDIs) was assessed using pooled HLMs (Supplemental Data). The potential for midostaurin, CGP52421, and CGP62221 to act as inducers of CYP3A4/5 enzymes was also evaluated in primary human hepatocytes of 3 individual donors using both mRNA quantification (real-time polymerase chain reaction) and CYP3A4/5 activity measurements (Supplemental Data). All of the in vitro enzyme activity was determined using liquid chromatography–tandem mass spectrometry (LC-MS/MS) of selective CYP3A4/5 probe substrate metabolism (Supplemental Data). The input parameters used for induction of CYP3A4, TDI, and reversible inhibition of CYP3A4/5 are summarized in Table 1.

Model Assumptions

Several assumptions were made for projection of human PK parameters. First, human F_a was set to 0.85 (see Absorption). Next, the fractions of total metabolism catalyzed by CYP3A4

DMD Fast Forward. Published on November 8, 2017 as DOI: 10.1124/dmd.117.078006
This article has not been copyedited and formatted. The final version may differ from this version.

in humans were estimated to be $fm_{CGP52421} \approx 0.37$, $fm_{CGP62221} \approx 0.37$, and $fm_{other\ 3A4} \approx 0.26$, with the assumptions that metabolite epimer structures were similar and that sequentially formed metabolites were equally contributed by primary and secondary metabolism. The CYP3A4/5 TDI K_I (total) was used. The CYP3A4 mRNA induction EC_{50} values of midostaurin, CGP52421, and CGP62221 were entered and optimized in the models (ie, 20-fold more potent than the experimental value). These modifications (ie, lower EC_{50} and fixed maximal induction [E_{max}]) were judged to be appropriate based on the very high plasma protein binding of all 3 components observed (> 99%); lower intracellular free concentrations in hepatocytes would be expected, which could reflect the amount of drug available for binding to the pregnane X receptor. The model was developed and verified using data from clinical studies in healthy subjects (further details follow). The disease- and/or age-related physiological changes affecting drug ADME properties, including enzyme activity and function, were not considered. Finally, the transporter-related drug interaction property was not included in the model.

Population

The simulations were performed using a simulated healthy volunteer population built in the Simcyp simulator, with individuals aged 20 to 55 years; the proportion of female subjects was set to 50%. The population size was 100, with 10 trials of 10 subjects per trial.

Simulation Trials

The simulated trials were run in a fasted state. The simulated trials for plasma PK of midostaurin and its 2 metabolites after single and multiple twice-daily (bid) doses are presented as follows. First, observed and predicted PK parameters and plasma concentration-time profiles of midostaurin, CGP52421, and CGP62221 following a single dose of midostaurin with a final market image (FMI) formulation of 50 mg in the simulated subjects were compared with those in

DMD Fast Forward. Published on November 8, 2017 as DOI: 10.1124/dmd.117.078006
This article has not been copyedited and formatted. The final version may differ from this version.

healthy volunteers in clinical studies. Control arms included food effect, relative bioavailability, DDIs with ketoconazole, and DDIs with rifampicin. Second, observed and predicted PK parameters and plasma concentration-time profiles of midostaurin, CGP52421, and CGP62221 following midostaurin (FMI) 75 mg bid on days 1 and 2 and 75 mg once daily (qd) on day 3 in the simulated subjects were compared with those in healthy volunteers in a cardiac intervals investigation. Third, observed and predicted PK parameters and plasma concentration-time profiles of midostaurin, CGP52421, and CGP62221 following midostaurin (FMI) 50 mg bid on days 1 to 6 and a single dose on day 7 in the simulated subjects were compared with those in healthy subjects with normal hepatic function in a PK study in subjects with impaired hepatic function.

PBPK Model Performance

The performance of the PBPK model was verified by comparing the simulated data with clinically observed DDIs. Input parameters for the PBPK model are in Supplemental Tables 10-15. The ketoconazole, rifampicin, and midazolam models available in the Simcyp compound library were used in the simulations. The simulated trials for plasma PK of midostaurin and its 2 metabolites in the presence of CYP3A4/5 inhibitors, a CYP3A4 inducer, or sensitive CYP3A4 substrates are shown in Table 2.

PBPK Model Development in Patients With AML and AdvSM

A PBPK model was also built to simulate the PK of midostaurin and its metabolites in patients with AML and advSM using a top-down approach. The model was mainly adopted from the previous Simcyp model in healthy subjects but with modifications. The assumption of these 2 patient models was that the protein binding, fm_{CYP3A4}, and in vitro DDI parameters of midostaurin and its metabolites were the same in patients and healthy subjects. The parameters

DMD Fast Forward. Published on November 8, 2017 as DOI: 10.1124/dmd.117.078006
This article has not been copyedited and formatted. The final version may differ from this version.

were updated based on the parameter estimated in the population (Pop) PK of midostaurin in patients with AML and advSM. These values were entered as described in the model for healthy subjects, with the exception of the following changes (Table 1**)**.

For patients with AML, parameters of distribution and elimination for midostaurin and parameters of elimination for CGP52421 were updated in the model for healthy subjects. V_{ss} of midostaurin was changed from 1 to 0.742 L/kg, with changes in parameters for Q (3 to 2.889 L/h) and V_{sac} (0.82 to 0.623 L/kg). CL_{int} of midostaurin was changed from ≈25.2 to 10.6 µL/min/mg/pmol of isoform. Accordingly, the midostaurin value of CL_{int} (in µL/min/pmol of CYP3A4) was assigned to the following CYP3A4 pathways: CGP52421 (37%) = 3.9; CGP62221 (37%) = 3.9; other (26%) = 2.8. For CGP52421, CL/F and CL_{int} were changed from 0.4 to 0.07 L/h and from 3.18 to 0.557 µL/min/mg/pmol of CYP3A4, respectively, with additional HLM clearance of 6.48 µL/min/mg of protein. Comparison of PBPK- and Pop PK–simulated data can be found in Supplemental Table 5, indicating that PBPK-simulated AUC and C_{max} values were within ≤ 2-fold of the values in the Pop PK data analysis.

For patients with advSM, parameters of absorption, distribution, and elimination for midostaurin were updated in the model for healthy subjects, so that the same V_{ss} and CL_{int} of midostaurin used in the model for patients with AML were used in the model for patients with advSM. In addition, midostaurin F_a was changed from 0.85 to 0.65, and the absorption rate constant was changed from 1.5 to 0.683 L/h. These values were updated based on optimization to best fit to population PK data in patients with advSM. Comparison of PBPK- and Pop PK–simulated data can be found in Supplemental Table 6, indicating that PBPK-simulated AUC and C_{max} values were within ≤ 2-fold of the values in the Pop PK data analysis.

DMD Fast Forward. Published on November 8, 2017 as DOI: 10.1124/dmd.117.078006
This article has not been copyedited and formatted. The final version may differ from this version.

PBPK Model Application

Following model verifications using data from clinical PK studies as well as clinical DDIs with ketoconazole, rifampicin, and midazolam in healthy subjects, the model was used to simulate hypothetical DDI scenarios at steady-state levels in healthy subjects and in patients with AML and advSM. These scenarios included (1) predicting the effect of moderate and strong CYP3A4 inhibitors and inducers on the exposure of midostaurin and its metabolites and (2) predicting the effect of midostaurin on the exposure of midazolam.

Simulation of the Effects of Moderate and Strong CYP3A4 Inhibitors and Inducers

The potential effects of CYP3A4 inhibitors fluconazole (moderate), itraconazole (strong), and ketoconazole (strong) and those of inducers efavirenz (moderate) and rifampicin (strong) on the PK of midostaurin and its metabolites were simulated. The Simcyp default PBPK models for efavirenz, fluconazole, itraconazole (fed capsule) with OH-itraconazole, ketoconazole, and rifampicin were used in these simulations. Next, midostaurin 50 mg bid was administered for 21 days; efavirenz 600 mg qd, fluconazole 200 mg qd, itraconazole 100 mg bid, ketoconazole 400 mg qd, or rifampicin 600 mg qd was co-administered with midostaurin for 7 days, starting on day 22. The effects of inhibitors and inducers on the PK of midostaurin were assessed after the last midostaurin dose on day 28.

Simulation of the Effects of Midostaurin and Its Metabolites on Midazolam

Due to a technical limitation in the current version of Simcyp, the model does not have the ability to enter midostaurin with 2 metabolites as perpetrators. Therefore, an alternative approach was used in which the simulations were performed using the perpetrator as the model's substrate and the victim as the model's inhibitor. Briefly, 2 simulations were conducted with midostaurin and its 2 metabolites in the substrate position and midazolam in the inhibitor

DMD Fast Forward. Published on November 8, 2017 as DOI: 10.1124/dmd.117.078006
This article has not been copyedited and formatted. The final version may differ from this version.

position. In the first simulation, the DDI properties of midostaurin and its metabolite CYP3A were turned off, representing the control PK of midazolam (in the absence of interaction). The second simulation was performed in the presence of midostaurin by including all the DDI properties, representing the interaction between midazolam as a perpetrator on midostaurin and its metabolites as victims. The exposure parameters [eg, area under the curve (AUC) and C_{max}] of midazolam from the first simulation were compared with those of the second simulation to determine the effect of midostaurin and its metabolites on midazolam. The dose regimen was midazolam 4 mg on day 28, with midostaurin 50 mg bid on days 1 to 28.

Plasma 4βHC Measurement

Study Design

Healthy adult volunteers aged 18 to 55 years were randomized to receive either rifampicin 600 mg (positive control) or placebo (negative control) from day 1 to 14. All individuals received midostaurin 50 mg on day 9. This unique, single administration was deemed not to interfere with the rifampicin-placebo effect. The positive control arm (n = 20) and negative control arm (n = 20) served as references for the progression of 4βHC levels. In a separate study, data from patients with advSM enrolled in an open-label, phase 2 study who received midostaurin 100 mg bid for 28 days (n = 10) were used to determine the 4βHC concentration profile. The study was conducted in accordance with the Declaration of Helsinki and approved by all relevant institutional review boards and ethics committees. The study design is summarized in Table 3.

Sample Collection and Analysis

To evaluate the plasma concentration of 4βHC, peripheral blood samples were collected on days 1 (baseline), 9 (before receiving midostaurin), 11, and 15 in the positive and negative

DMD Fast Forward. Published on November 8, 2017 as DOI: 10.1124/dmd.117.078006
This article has not been copyedited and formatted. The final version may differ from this version.

control arms (healthy participants in a clinical DDI study with rifampicin) and on days 1, 3, 8, 15, 22, and 28 of cycle 1 in the patient study. The plasma concentration of 4βHC was measured as described (Diczfalusy et al., 2011), using validated LC-MS/MS with a lower limit of quantification of 3 ng/mL.

Statistical Analyses

Statistical analyses were descriptive only; no formal statistical tests were performed. Only subjects with an available full 4βHC profile were included in the analysis. For each subject, values at each time point and percent change from baseline were considered and median values were computed (data not shown); the mean and GM of the individual value from baseline were also calculated. Results were plotted to visually represent the data and support the interpretations.

RESULTS

Simulated and Observed PK Following Single and Multiple Doses of Midostaurin in Healthy Subjects

A Simcyp model was established to predict the PK of midostaurin, CGP52421, and CGP62221 after single (50 mg) and multiple (50 or 75 mg) oral doses in healthy subjects. Simulated PK profiles were compared with data from several clinical trials in which single-agent PK was available. Overall, the PK of midostaurin, CGP52421, and CGP62221 was predicted reasonably well. The simulated mean plasma concentration-time profiles with observed data overlaid are shown in Figure 1. The representative tabulated simulated and actual PK parameters for midostaurin, CGP52421, and CGP62221 following a single dose of 50 mg and 50 mg BID of midostaurin can be found in Supplemental Tables 7 and 8.

DMD Fast Forward. Published on November 8, 2017 as DOI: 10.1124/dmd.117.078006
This article has not been copyedited and formatted. The final version may differ from this version.

Simulated and Observed DDIs With CYP3A4 Inhibitor Ketoconazole and Inducer Rifampicin in Healthy Subjects

The clinical DDI trial of midostaurin 50 mg with ketoconazole 400 mg qd or rifampicin 600 mg qd was simulated according to the clinical trial design in healthy subjects. Simulated profiles for the interaction of midostaurin and ketoconazole or midostaurin and rifampicin were then compared with observed data, as shown in Figure 2.

The predicted and observed midostaurin AUC GM ratios (GMRs) were 5.8 (AUC_{inf}, 6.3) and 6.1 (AUC_{inf}, 10.4), respectively, and the predicted and observed C_{max} GMRs were 2.1 and 1.8, respectively, when midostaurin was co-administered with ketoconazole. For CGP52421, the predicted and observed GMRs were 0.6 and 1.2 for AUC and 0.4 and 0.5 for C_{max}, respectively. For CGP62221, the predicted and observed GMRs were 0.6 and 1.0 for AUC and 0.3 and 0.6 for C_{max}, respectively. When midostaurin was co-administered with rifampicin, the predicted vs observed decrease in GM AUC and C_{max} for midostaurin was 90% vs 94% and 79% vs 73%, respectively. The predicted vs observed decrease in GM AUC for CGP52421 was 65% vs 59%, respectively, and for CGP622221, 55% vs 92%, respectively. The corresponding predicted vs observed decrease in GM C_{max} for CGP52421 and CGP62221 was 9% vs 35% and 37% vs no change, respectively. Overall, the model predicted the exposure change in midostaurin reasonably well when it was co-administered with ketoconazole or rifampicin. However, for its metabolites, there was a trend toward underprediction of exposure change compared with observed data (Table 4).

DMD Fast Forward. Published on November 8, 2017 as DOI: 10.1124/dmd.117.078006
This article has not been copyedited and formatted. The final version may differ from this version.

Simulated DDIs With Moderate and Strong CYP3A4 Inhibitors and Inducers at Steady State in Healthy Subjects and Patients With AML and AdvSM

The potential effects of CYP3A4 inhibitors fluconazole (moderate), itraconazole (strong), and ketoconazole (strong) as well as those of CYP3A4 inducers efavirenz (moderate) and rifampicin (strong) on midostaurin exposure at steady-state levels (50 mg bid for healthy subjects and patients with AML and 100 mg bid for patients with advSM for 28 days) were simulated both in healthy subjects and in patients with AML and advSM.

GMRs of $AUC_{0\text{-}tau}$ for itraconazole were predicted to be 2.5-, 1.3-, and 1.3-fold for midostaurin, CGP52421, and CGP62221, respectively, using the model for healthy subjects. GMR values of $AUC_{0\text{-}tau}$ for ketoconazole DDIs were predicted to be 5.4-, 1.6-, and 1.7-fold for midostaurin, CGP52421, and CGP62221, respectively. The results indicated that the impact of DDIs after multiple doses of midostaurin (to steady state) with ketoconazole was similar to the impact of DDIs after a single midostaurin dose (Table 4). GMR values of $AUC_{0\text{-}tau}$ for midostaurin with fluconazole were predicted to be 2.7-, 1.6-, and 1.5-fold for midostaurin, CGP52421, and CGP62221, respectively. GMR values of $AUC_{0\text{-}tau}$ for rifampicin DDIs were predicted to decrease by 43%, 30%, and 25% for midostaurin, CGP52421, and CGP62221, respectively. The impact of DDIs after multiple doses of midostaurin (to steady state) with rifampicin appears to be less than the impact of DDIs after a single dose of midostaurin (Table 4). With co-administration of efavirenz, GMR values of $AUC_{0\text{-}tau}$ were predicted to decrease by 8%, 5%, and 4% for midostaurin, CGP52421, and CGP62221, respectively, suggesting a minimal impact on exposure to midostaurin and its metabolites. The overall prediction results are summarized in the forest plots shown in Figure 3.

DMD Fast Forward. Published on November 8, 2017 as DOI: 10.1124/dmd.117.078006
This article has not been copyedited and formatted. The final version may differ from this version.

GMR values of $AUC_{0\text{-}tau}$ for itraconazole for AML and advSM were predicted to be 2.2- and 2.0-fold, 1.0- and 1.2-fold, and 1.2-fold for midostaurin, CGP52421, and CGP62221, respectively, applying the models for patients with AML and advSM. GMR values of $AUC_{0\text{-}tau}$ for ketoconazole DDIs for AML and advSM were predicted to be 4.2- and 4.4-fold, 1.1- and 1.5-fold, and 1.5- and 1.6-fold for midostaurin, CGP52421, and CGP62221, respectively. GMR values of $AUC_{0\text{-}tau}$ for midostaurin with fluconazole for AML and advSM were predicted to be 2.5- and 2.6-fold, 1.2- and 1.6-fold, and 1.5- and 1.6-fold for midostaurin, CGP52421, and CGP62221, respectively. GMR values of $AUC_{0\text{-}tau}$ for rifampicin DDIs for AML and advSM were predicted to decrease by 27% and 34%%, 13% and 24%, and 21% and 20% for midostaurin, CGP52421, and CGP62221, respectively. With co-administration of efavirenz, GMR values of $AUC_{0\text{-}tau}$ were predicted to decrease by 5% and 3%, 1% and 2%, and 3% and 2% for midostaurin, CGP52421, and CGP62221, respectively. The overall prediction results are summarized in the forest plots shown in Figure 3.

Simulated Hepatic CYP3A4 Dynamics After Treatment With CYP3A4 Inhibitors and Inducers

From a victim DDI perspective, the model reasonably predicted the observed changes in midostaurin exposure with ketoconazole and rifampicin. The qualified model for healthy subjects was then applied to predict the DDI effect with ketoconazole or rifampicin at steady-state levels. In the presence of a strong CYP3A4 inducer (rifampicin 600 mg qd), the ratios (relative to the control arm) of maximal increased hepatic CYP3A4 activity were 4.9 and 1.9 after a single dose and bid dosing of midostaurin (steady state), respectively (Figure 4A). These ratios are consistent with predicted reductions of midostaurin exposure by 90% (single dose) and 43% (steady state) due to the change in CYP3A4 enzyme activity. Conversely, in the presence of a strong CYP3A4

DMD Fast Forward. Published on November 8, 2017 as DOI: 10.1124/dmd.117.078006
This article has not been copyedited and formatted. The final version may differ from this version.

inhibitor (ketoconazole 400 mg qd), the ratios (relative to the control arm) of maximal increased hepatic CYP3A4 activity were 1.08 and 1.02 after a single dose and bid dosing of midostaurin (steady state), respectively (Figure 4B). These ratios are consistent with predicted similar increases of midostaurin exposure by 5.8-fold (single dose) and 5.4-fold (steady state) due to the similar change in CYP3A4 enzyme activity.

Simulated and Observed DDIs With CYP3A4 Substrate Midazolam

The clinical combination trial for a single dose of midazolam (4 mg) with a single dose of midostaurin (100 mg on day 1, followed by 50 mg bid on days 2 to 4) was simulated according to the clinical trial design. The effect of midostaurin on midazolam $AUC_{0\text{-}inf}$ was predicted to be 1.2-fold (observed, 1.0-fold) and 0.74-fold (observed, 0.95-fold) on days 1 and 6, respectively. The corresponding change in midazolam C_{max} was predicted to be 1.2-fold (observed, 0.8-fold) and 1-fold (observed, 0.9-fold), respectively. These results indicated that no CYP3A4 induction effect could be detected in a relatively short study duration. The study duration was short due to safety concerns for healthy subjects. The observed and simulated plasma concentration-time profiles are presented in Figure 5.

Simulated DDIs With CYP3A4 Substrate Midazolam at Steady State in Healthy Subjects and Patients With AML and AdvSM

Simcyp Simulation

The potential interaction of midostaurin with the sensitive CYP3A4 substrate midazolam under steady-state midostaurin dosing conditions was simulated in both healthy subjects and patients with AML and advSM. With co-administration of midostaurin (50 mg bid in healthy subjects) to steady state (ie, 28 days), midazolam AUC_{inf} and C_{max} ratios (relative to dose alone) were predicted to be 0.59 (decreased by 41%) and 0.78 (decreased by 22%), respectively (Figure

DMD Fast Forward. Published on November 8, 2017 as DOI: 10.1124/dmd.117.078006
This article has not been copyedited and formatted. The final version may differ from this version.

6). The net decrease in midazolam exposure (AUC_{inf}) in the presence of midostaurin (50 or 100 mg bid in AML and advSM, respectively) relative to dose alone was predicted to be 0.60 and 0.54, respectively. Overall, this would be indicative of an induction effect of midostaurin and its metabolites at steady state.

Assessment of CYP3A4 Activity Using Plasma Biomarker 4βHC Levels

At baseline, the GM 4βHC levels were similar between the negative control arm, positive control arm, and midostaurin arm despite the absence of global randomization **(**Table 5**)**.

In the negative control arm (subjects receiving placebo), 4βHC levels remained stable on days 9, 11, and 15. No time dependency in levels was observed. In contrast, 4βHC levels notably increased over time in the positive control arm (subjects treated with rifampicin) on days 9, 11, and 15.

In the midostaurin arm (100 mg bid), 4βHC levels moderately increased (≈ 1.8-fold) until day 15, at which point they had approximately doubled relative to baseline. The 4βHC levels remained constant from day 15 to PK steady state of midostaurin (day 28) (Figure 7). GM 4βHC levels on days 3, 8, 9, 11, 15, 22, and 28 are presented (Table 5). A net increase in plasma 4βHC was observed with midostaurin (100 mg bid) under steady-state conditions, also suggesting an induction effect of midostaurin and its metabolites at steady state. In the rifampicin arm (positive control), the 4βHC levels increased 3.2-, 3.5-, and 4.3-fold on days 9, 11, and 15, respectively.

DISCUSSION

In the current study, we present a case example using a PBPK modeling approach to predict the DDIs associated with a mixed net effect (TDI and induction) on CYP3A4 for the parent compound as well as its 2 major circulating metabolites in healthy subjects and in patients with AML and advSM.

DMD Fast Forward. Published on November 8, 2017 as DOI: 10.1124/dmd.117.078006
This article has not been copyedited and formatted. The final version may differ from this version.

In our modeling approach, in vitro study–determined parameters (Supplemental Data) were initially used. However, the simulated concentration-time profiles after multiple dosing showed net auto-inhibition (data not shown) rather than observed auto-induction. Subsequently, EC_{50} values were optimized (20-fold more potent for all 3 components) based on fitting of single- and multiple-dosing PK profiles from clinical PK and DDI trials. The under-prediction in induction magnitude using in vitro data could be due to other mechanisms involved in the induction of CYP3A4 mRNA. For example, CYP3A4 could be induced through P53 protein activation and may be relevant for patients with cancer (Goldstein et al., 2013; Harmsen et al., 2008; Elias et al., 2013); tyrosine kinase inhibitors may potentially induce CYP3A4 mRNA involving CAR1 and P53 (Lin et al., 2016). Because the induction was ultimately modeled using a "top-down" approach for midostaurin and its metabolites, any other potential mechanisms of CYP3A4 regulation would be captured in the model. Although a more extensive data set was required, this model is considered to be mechanistic because it allows for incorporation of changes in clearance of midostaurin as a result of its auto-inhibition/induction after multiple dosing. By using the middle-out approach (combining top-down and bottom-up), the model could reasonably capture the acute effects of auto-inhibition and subsequent auto-induction, as predicted by increased exposure of midostaurin on day 7 relative to day 1 followed by a decreasing trend in exposure on day 28. The half-life and time to steady state were taken into account, and a standard dosing regimen (50 mg bid for healthy subjects and patients with AML and 100 mg bid for patients with advSM for 28 days) was consistently used to closely mimic a potential clinical, steady-state dosing regimen. The model was then used to simulate the PK profiles of midostaurin and its metabolites at steady state and predict the subsequent effects on midazolam exposure.

DMD Fast Forward. Published on November 8, 2017 as DOI: 10.1124/dmd.117.078006
This article has not been copyedited and formatted. The final version may differ from this version.

Per regulatory guidance (FDA, 2012; EMA, 2012), the simulated midazolam AUC ratio is consistent with the classification of midostaurin as a weak CYP3A4 inducer (20%-50% decrease in AUC). The simulated net effect of midostaurin and its metabolites as a weak CYP3A4 inducer was also supported by changes in plasma 4βHC, an emerging biomarker of CYP3A4 activity (Bjorkhem-Bergman et al., 2013; Bodin et al., 2001; Leil et al., 2014). The net effect was an increase in observed 4βHC, suggesting CYP3A4 induction. Based on the relationships between midazolam AUC GMR, rifampicin dose, and plasma 4βHC, a framework has been developed recently to classify the CYP3A4 inducer potencies of new chemical entities after 14 days of dosing (Mangold et al., 2016). Using this framework (although not accepted currently by regulatory authorities) and considering the observed increase in plasma 4βHC in our study (maximal 2-fold increase), midostaurin (100 mg bid for 28 days) could be viewed as a moderate CYP3A4 inducer in the worst-case scenario. One caveat to using the plasma 4βHC biomarker is that the potency classification can be dependent on sample size. Based on the low variability of 4βHC, it is theorized that for a strong inducer such as rifampicin, there would be at least an 80% probability of detecting a 4βHC elevation with a sample size of < 10. For detecting moderate and weak inducers, the approximate sample size would be $n = 10$ to 25 and $n > 60$, respectively (Leil et al., 2014). Given that the 4βHC data with midostaurin are based on only 10 patients, the classification of midostaurin as a weak to moderate CYP3A4 inducer is, at best, supportive of the PBPK modeling results and needs further confirmation using a larger sample size. Nonetheless, the 4βHC biomarker data provided an additional tool to evaluate the net effect of CYP3A4 induction or inhibition by midostaurin and its metabolites at steady state when midostaurin was co-administered with midazolam and increased our confidence in the DDI predictions.

DMD Fast Forward. Published on November 8, 2017 as DOI: 10.1124/dmd.117.078006
This article has not been copyedited and formatted. The final version may differ from this version.

To evaluate the victim DDI potential of midostaurin, the CYP3A4 activity after single and multiple doses of midostaurin needs to be considered. The change in simulated CYP3A4 activity with midostaurin alone and in combination with ketoconazole was similar in both single- and multiple-dose scenarios (Figure 4B). Based on this observation, CYP3A4 inhibitors are predicted to have a similar impact on midostaurin exposure under single- and multiple-dose conditions.

However, the DDI predictions in the presence of CYP3A4 inducers were found to be highly dependent on single- vs multiple-dose conditions. As expected, CYP3A4 activity was not significantly affected by single-dose midostaurin, but it increased upon multiple dosing. Consequently, when another CYP3A4 inducer (rifampicin) was co-administered, the net increase in CYP3A4 activity was less with a single dose than with multiple midostaurin doses, resulting in a 90% decrease in midostaurin exposure under single-dose conditions vs a 43% decrease under multiple-dose conditions. For these reasons, efavirenz (a moderate CYP3A4 inducer) was predicted to have a minimal impact on midostaurin exposure at steady state (ie, a decrease of 8%).

It is noticed that the predicted increase in the AUC of midostaurin after co-administration of itraconazole 100 mg bid was lower than that with ketoconazole 400 mg qd. This is likely in part due to the metabolism of itraconazole as a CYP3A4 substrate being affected by midostaurin and its metabolites, resulting in the induction of CYP3A4 activity. The exposure of itraconazole in the presence of midostaurin was predicted to be lower than for itraconazole administered alone, and the inhibitory effect of itraconazole metabolites appears to be less potent than that of itraconazole alone.

DMD Fast Forward. Published on November 8, 2017 as DOI: 10.1124/dmd.117.078006
This article has not been copyedited and formatted. The final version may differ from this version.

Our simultaneous PBPK modeling approach takes the first step toward assessing the complex CYP3A4 DDI potential of a parent drug and its 2 metabolites in healthy subjects. In order to assess the DDI potential of other CYP3A4 inhibitors/inducers used routinely in patients with cancer, two additional PBPK models were built for patients with AML and advSM. Patients with cancers are different than healthy subjects in terms of demographic and physiological properties. Moreover, the population of patients with cancer is heterogeneous, and the differences in various characteristics for patients with cancer, as well as different types of cancer (eg, AML and advSM), can affect the ADME and PK of drugs. To fully characterize physiological differences between healthy subjects and patients with cancer, development of a cancer population file has been shown to be a promising tool for the prediction of PK in patients (Cheeti et al., 2013). However, development, validation, and application of cancer-specific profiles will require more comprehensive data collection. Due to the limited knowledge and understanding of the mechanisms of the PK differences observed in healthy subjects and patients with cancer, two individual compound files were built for patients with AML and patients with advSM; the lower V_{ss} and CL_{int} of midostaurin for patients with both cancer and lower clearance of CGP52421 for AML compared with the model for healthy subjects were applied to the patient models. Lower clearances of midostaurin and CGP52421 in patients with AML than in healthy subjects are likely due to multiple factors. The mechanism of the differences in these parameters is not clear; however, it may be a difference in midostaurin distribution (although similar plasma protein binding between healthy subjects and patients was observed in ex vivo studies) and metabolic clearance between the two populations. It could also be that the metabolic clearance of CGP52421 in patients with AML is different than that in healthy subjects and patients with advSM. In recent years, researchers have suggested that circulating levels of cytokines, including

DMD Fast Forward. Published on November 8, 2017 as DOI: 10.1124/dmd.117.078006
This article has not been copyedited and formatted. The final version may differ from this version.

IL-6, are significantly higher in patients with AML than in healthy subjects (Tsimberidou et al., 2008; Meyers et al., 2005). Furthermore, suppression of CYP3A4 by IL-6 in hepatocytes was observed and clinical examples have been reported showing that CYP3A4-mediated metabolism was affected by cytokine modulators (eg, elevation of IL-6 level), resulting in reduced CYP3A4 expression (Evers et al., 2013). In addition, a lower F_a of midostaurin than those in the healthy subject model was used for the advSM model. The reduced overall absorption in patients with advSM could be due to the disease-related abnormal numbers of mast cells in organs, including the gastrointestinal tract (Cardet et al., 2013), which may affect oral absorption.

In conclusion, the PBPK model described here using a middle-out approach reasonably predicted PK profiles of midostaurin and its 2 metabolites after single and multiple dosing. The simultaneous parent and metabolite modeling approach allowed predictions under steady-state conditions that were not possible to achieve in healthy subjects. The model also captured the apparent effect of mixed TDI/induction mechanisms. Our combined, multipronged approach allowed the extension of findings from single-dose clinical DDI studies and enabled predictions of steady-state DDI effects to be made with improved confidence. The results generated using this integrated approach provide support of clinical recommendations and potential product label language.

ACKNOWLEDGMENTS

The data analysis of 4βHC was conducted by statistician Matthieu Villeneuve, a former employee of Novartis. Medical editorial assistance was provided by Jennifer Gooch, PhD, and Pamela Tuttle, PhD, CMPP, of ArticulateScience LLC. Funding for medical editorial assistance was provided by Novartis Pharmaceuticals Corporation.

DMD Fast Forward. Published on November 8, 2017 as DOI: 10.1124/dmd.117.078006
This article has not been copyedited and formatted. The final version may differ from this version.

AUTHORSHIP CONTRIBUTIONS

Participated in research design: Gu, Dutreix, Einolf, He

Conducted experiments: Gu, Chun, Wang

Performed data analysis: Gu, Dutreix, Villeneuve

Contributed to the writing of the manuscript: Gu, Rebello, Dutreix, Einolf, He, Ouatas

REFERENCES

Andrejauskas-Buchdunger E and Regenass U (1992) Differential inhibition of the epidermal growth factor-, platelet-derived growth factor-, and protein kinase C-mediated signal transduction pathways by the staurosporine derivative CGP 41251. *Cancer Res* **52**: 5353–5358.

Barry EV, Clark JJ, Cools JV, Roessel J, and Gilliland DG (2007) Uniform sensitivity of FLT3 activation loop mutants to the tyrosine kinase inhibitor midostaurin. *Blood* **110**: 4476–4479.

Bjorkhem-Bergman L, Bäckström T, Nylén H, Rönquist-Nii Y, Bredberg E, Andersson TB, Bertilsson L, and Diczfalusy U (2013) Comparison of endogenous 4beta-hydroxycholesterol with midazolam as markers for CYP3A4 induction by rifampicin. *Drug Metab Dispos* **41**: 1488–1493.

Bodin K, Bretillon L, Aden Y, Bertilsson L, Broomé U, Einarsson C, and Diczfalusy U (2001) Antiepileptic drugs increase plasma levels of 4beta-hydroxycholesterol in humans: evidence for involvement of cytochrome p450 3A4. *J Biol Chem* **276**: 38685–38689.

Cardet JC, Akin C, and Lee MJ (2013) Mastocytosis: update on pharmacotherapy and future directions. *Expert Opin Pharmacother* **14**: 2033–2045.

Cheeti S, Budha NR, Rajan S, Dresser MJ, and Jin JY (2013) A physiologically based pharmacokinetic (PBPK) approach to evaluate pharmacokinetics in patients with cancer. *Biopharm Drug Dispos* **34**: 141–154.

Committee for Human Medicinal Products (2012) *Guideline on the Investigation of Drug Interactions.* European Medicines Agency, London.

Diczfalusy U, Nylen H, Elander P, and Bertilsson L (2011) 4beta-hydroxycholesterol, an endogenous marker of CYP3A4/5 activity in humans. *Br J Clin Pharmacol* **71**: 183–189.

Dutreix C, Munarini F, Lorenzo S, Roesel J, and Wang Y (2013) Investigation into CYP3A4-mediated drug-drug interactions on midostaurin in healthy volunteers. *Cancer Chemother Pharmacol* **72**: 1223–1234.

Dutreix C, Sebastien L, and Wang Y (2014) Comparison of two endogenous biomarkers of CYP3A4 activity in a drug-drug interaction study between midostaurin and rifampicin. *Eur J Clin Pharmacol* **70**: 915–920.

Elias A, Wu J, Chen T (2013). Tumor suppressor protein p53 negatively regulates human pregnane X receptor activity. *Mol Pharmacol* 8**3**: 1229–1236.

European Medicine Agency (EMA), Committee for Human Medicinal Products (CHMP) Guideline on the investigation of drug interactions. 21 June 2012.

Fabbro D, Ruetz S, Bodis S, Pruschy M, Csermak K, Man A, Campochiaro P, Wood J, O'Reilly T, and Meyer T (2000) PKC412: a protein kinase inhibitor with a broad therapeutic potential. *Anticancer Drug Des* **15**: 17–28.

Fahmi OA, Hurst S, Plowchalk D, Cook J, Guo F, Youdim K, Dickins M, Phipps A, Darekar A, Hyland R, and Obach RS (2009) Comparison of different algorithms for predicting clinical drug–drug interactions, based on the use of CYP3A4 in vitro data: predictions of compounds as precipitants of interaction. *Drug Metab Dispos* **37**: 1658–1666.

FDA Guidance for Industry (2012) Drug Interaction Studies—Study Design, Data Analysis, Implications for Dosing, and Labeling Recommendations. US Department of Health and Human Services, Food and Drug Administration, Center for Drug Evaluation and Research, Center for Veterinary Medicine, Rockville, MD.

Fenneteau F, Poulin P, and Nekka F (2010) Physiologically based predictions of the impact of inhibition of intestinal and hepatic metabolism on human pharmacokinetics of CYP3A substrates. *J Pharm Sci* **99**: 486–514.

Fischer T, Stone RM, Deangelo DJ, Galinsky I, Estey E, Lanza C, Fox E, Ehninger G, Feldman EJ, Schiller GJ, Klimek VM, Nimer SD, Gilliland DG, Dutreix C, Huntsman-Labed A, Virkus J, and Giles FJ (2010) Phase IIB trial of oral midostaurin (PKC412), the FMS-like tyrosine kinase 3 receptor (FLT3) and multi-targeted kinase inhibitor, in patients with acute myeloid leukemia and high-risk myelodysplastic syndrome with either wild-type or mutated FLT3. *J Clin Oncol* **28**: 4339–4345.

Galetin A, Burt H, Gibbons L, and Houston JB (2006) Prediction of time-dependent CYP3A4 drug–drug interactions: impact of enzyme degradation, parallel elimination pathways, and intestinal inhibition. *Drug Metab Dispos* **34**: 166–175.

Gallogly MM and Lazarus HM (2016) Midostaurin: an emerging treatment for acute myeloid leukemia patients. *J Blood Metabol* **7**: 73–83.

Garg V, Chandorkar G, Farmer HF, Smith F, Alves K, and van Heeswijk RP (2012) Effect of telaprevir on the pharmacokinetics of midazolam and digoxin. *J Clin Pharmacol* **52**: 1566–1573.

Goldstein I, Rivlin N, Shoshana OY, Ezra O, Madar S, Goldfinger N, Rotter V (2013). Chemotherapeutic agents induce the expression and activity of their clearing enzyme CYP3A4 by activating p53. *Carcinogenesis* **34**: 190–198.

Gotlib J, Berube C, Growney JD, Smith F, Alves K, and van Heeswijk RP (2005) Activity of the tyrosine kinase inhibitor PKC412 in a patient with mast cell leukemia with the D816V KIT mutation. *Blood* **106**: 2865–2870.

Gotlib J, Kluin-Nelemans H, George TI, Akin C, Sotlar K, Hermine O, Awan FT, Hexner E, Mauro MJ, Sternberg DW, Villeneuve M, Huntsman Labed A, Stanek EJ, Hartmann K, Horny HP, Valent P, and Reiter A (2016) Efficacy and safety of midostaurin in advanced systemic mastocytosis. *N Engl J Med* **374**: 2530–2541.

Harmsen S, Meijerman I, Beijnen JH, Schellens JH (2008). Nuclear receptor mediated induction of cytochrome P450 3A4 by anticancer drugs: a key role for the pregnane X receptor. Cancer *Chemother Pharmacol* **64**: 35–43.

He H, Tran P, Gu H, Tedesco V, Zhang J, Lin W, Gatlik E, Klein K, and Heimbach T (2017) Midostaurin, a novel protein kinase inhibitor for the treatment of acute myelogenous leukemia: insights from human absorption, metabolism, and excretion studies of a BDDCS II drug. *Drug Metab Dispos* **45**: 540–555.

Leil TA, Kasichayanula S, Boulton DW, and LaCreta F (2014) Evaluation of 4beta-hydroxycholesterol as a clinical biomarker of CYP3A4 drug interactions using a Bayesian mechanism-based pharmacometric model. *CPT Pharmacometrics Syst Pharmacol*. **3**: e120.

Levis M, Brown P, Smith D, Stine A, Pham R, Stone R, Deangelo D, Galinsky I, Giles F, Estey E, Kantarjian H, Cohen P, Wang Y, Roesel J, Karp JE, and Small D (2006) Plasma inhibitory activity (PIA): a pharmacodynamic assay reveals insights into the basis for cytotoxic response to FLT3 inhibitors. *Blood* **18**: 3477–3483.

Lin Z, Fahmi OA, Johnson N, Rodrigues DA, Obach RS, Steyn SJ, Zientek M, and Goosen TC. (2016) Tyrosine kinase inhibitors robustly induced CYP3A4 mRNA, but not activity via multiple pathways. Poster presented at: 21st International Symposium on Microsomes and Drug Oxidations; October 2–6, 2016; Davis, CA.

Mangold JB, Wu F, and Rebello S (2016) Compelling relationship of CYP3A induction to levels of the putative biomarker 4β-hydroxycholesterol and changes in midazolam exposure. *Clin Pharm Drug Develop* **5**: 245–249.

Meyers CA, Albitar M, Estey E (2005). Cognitive impairment, fatigue, and cytokine levels in patients with acute myelogenous leukemia or myelodysplastic syndrome. *Cancer* **104**: 788–793.

Propper DJ, McDonald AC, Man A, Thavasu P, Balkwill F, Braybrooke JP, Caponigro F, Graf P, Dutreix C, Blackie R, Kaye SB, Ganesan TS, Talbot DC, Harris AL, and Twelves C (2001) Phase I and pharmacokinetic study of PKC412, an inhibitor of protein kinase C. *J Clin Oncol* **19**: 1485–1492.

Prueksaritanont T, Chu X, Gibson C, Cui D, Yee KL, Ballard J, Cabalu T, and Hochman J (2013) Drug–drug interaction studies: regulatory guidance and an industry perspective. *AAPS J* **15**: 629–645.

Reitman ML, Chu X, Cai X, Yabut J, Venkatasubramanian R, Zajic S, Stone JA, Ding Y, Witter R, Gibson C, Roupe K, Evers R, Wagner JA, and Stoch A (2011) Rifampin's acute inhibitory and chronic inductive drug interactions: experimental and model-based approaches to drug–drug interaction trial design. *Clin Pharmacol Ther* **89**: 234–242.

Stone RM, DeAngelo DJ, Klimek V, Galinsky I, Estey E, Nimer SD, Grandin W, Lebwohl D, Wang Y, Cohen P, Fox EA, Neuberg D, Clark J, Gilliland DG, and Griffin JD (2005) Patients with acute myeloid leukemia and an activating mutation in FLT3 respond to a small-molecule FLT3 tyrosine kinase inhibitor, PKC412. *Blood* **105**: 54–60.

Stone RM, Mandrekar S, Sandord, L, Geyer S, Bloomfield CD, Döhner K, Thiede C, Marcucci G, Lo-Coco F, Klisovic RB, Wei A, Sierra J, Sanz MA, Brandwein JM, de Witte T,

Niederwieser D, Appelbaum FR, Medeiros BC, Tallman MS, Krauter J, Schlenk RF, Ganser A, Serve H, Ehninger G, Amadori S, Larson RA, and Döhner H (2015) The multi-kinase inhibitor midostaurin (M) prolongs survival compared with placebo (P) in combination with daunorubicin (D)/cytarabine (C) induction (ind), high-dose C consolidation (consol), and as maintenance (maint) therapy in newly diagnosed acute myeloid leukemia (AML) patients (pts) age 18-60 with FLT3 mutations (muts): an international prospective randomized (rand) P-controlled double-blind trial (CALGB 10603/RATIFY [Alliance]). *Blood* **126**: abstract 6.

Tsimberidou AM, Estey E, Wen S, Pierce S, Kantarjian H, Albitar M, Kurzrock R (2008). The prognostic significance of cytokine levels in newly diagnosed acute myeloid leukemia and high-risk myelodysplastic syndromes. *Cancer* **113**: 1605–1613.

Wang Y, Yin OQ, Graf P, Kisicki JC, and Schran H (2008) Dose- and time-dependent pharmacokinetics of midostaurin in patients with diabetes mellitus. *J Clin Pharmacol* **48**: 763–775.

Weisberg E, Boulton C, Kelly LM, Manley P, Fabbro D, Meyer T, Gilliland DG, and Griffin JD (2002) Inhibition of mutant FLT3 receptors in leukemia cells by the small molecule tyrosine kinase inhibitor PKC412. *Cancer Cell* **1**: 433–443.

Weiss HM, Gatlik E (2014). Equilibrium gel filtration to measure plasma protein binding of very highly bound drugs. *J Pharm Sci*. **103**:752-759.

Yeo KR, Walsky RL, Jamei M, Rostami-Hodjegan A, and Tucker GT (2011) Prediction of time-dependent CYP3A4 drug–drug interactions by physiologically based pharmacokinetic modelling: impact of inactivation parameters and enzyme turnover. *Eur J Pharm Sci* **43**: 160–173.

Yin OQ, Wang Y, and Schran H (2008) A mechanism-based population pharmacokinetic model for characterizing time-dependent pharmacokinetics of midostaurin and its metabolites in human subjects. *Clin Pharmacokinet* **47**: 807–816.

DMD Fast Forward. Published on November 8, 2017 as DOI: 10.1124/dmd.117.078006
This article has not been copyedited and formatted. The final version may differ from this version.

FOOTNOTES

Funding for this project was provided by Novartis.

DMD Fast Forward. Published on November 8, 2017 as DOI: 10.1124/dmd.117.078006
This article has not been copyedited and formatted. The final version may differ from this version.

FIGURE LEGENDS

Figure 1. The black lines represent the simulated mean plasma concentration-time profiles of midostaurin (panels A, D, and G), CGP52421 (panels B, E, and H), and CGP62221 (panels C, F, and I). The dashed lines represent the simulated lower 5th and upper 95th percentiles. The symbols and error bars represent the observed mean plasma concentration-time data and standard deviation from 2 clinical trials (A2111 and A2108) and 2 control trials (A2109 and A2110) for panels A, B, and C. All 4 trials were open-label, randomized, parallel-group studies in healthy volunteers. Panels A, B, and C show day 1 following midostaurin 50 mg; panels D, E, and F show days 1 to 3 following midostaurin 75 mg twice daily for 3 days; and panels G, H, and I show days 1 and 7 following midostaurin 50 mg twice daily for 6 days and a single dose on day 7.

Figure 2. The simulated mean plasma concentration-time profiles of midostaurin after treatment with midostaurin 50 mg (A) on day 6 in the absence (solid line) or presence (dashed line) of ketoconazole 400 mg once daily on days 1 to 10 and (B) on day 9 in the absence (solid line) or presence (dashed line) of rifampicin 600 mg once daily on days 1 to 14. The symbols (with and without interaction in red and purple, respectively) and error bars represent the observed mean plasma concentration-time data and standard deviation, respectively.

Figure 3. Simulated area under the curve (AUC) and maximum concentration (C_{max}) ratios (with 90% CIs) in healthy volunteers (HVs) and in patients with acute myeloid leukemia (AML) and advanced systemic mastocytosis (advSM) for (A) midostaurin, (B) CGP52421, and (C) CGP62221 when co-administered with ketoconazole, itraconazole, fluconazole, efavirenz, and rifampicin. The open circles and closed squares represent geometric mean C_{max} and AUC ratios, respectively.

DMD Fast Forward. Published on November 8, 2017 as DOI: 10.1124/dmd.117.078006
This article has not been copyedited and formatted. The final version may differ from this version.

Figure 4. (A) The solid green and red lines represent the simulated cytochrome P450 3A4 (CYP3A4) hepatic activity (% of baseline) after a 50-mg single dose and a 50-mg twice-daily dose of midostaurin to steady state (day 28), respectively, after treatment with rifampicin 600 mg once daily. (B) The solid green and red lines represent the simulated CYP3A4 hepatic activity (% of baseline) after a 50-mg single dose and a 50-mg twice-daily dose of midostaurin to steady state (day 28), respectively, after treatment with ketoconazole 400 mg once daily.

Figure 5. The solid lines represent the simulated mean systemic plasma concentration-time profiles of midazolam 4 mg (A) in the absence of midostaurin, (B) with a single dose of midostaurin 100 mg on day 1, and (C) with an additional twice-daily dose of midostaurin 50 mg on days 2 to 4. The dashed lines represent the simulated lower 5th and upper 95th percentiles. The symbols (with and without interaction in red and purple, respectively) and error bars represent the observed mean plasma concentration-time data and standard deviation, respectively.

Figure 6. The lines represent the mean plasma concentration-time profiles of (A) midazolam, (B) midostaurin, (C) CGP52421, and (D) CGP62221 following co-administration of midazolam 4 mg and midostaurin 50 mg twice daily for 28 days.

Figure 7. Overlays of measured 4β-hydroxycholesterol (4βHC) profiles with ratios relative to baseline and predicted changes in midazolam area under the curve (AUC) ratios affected by midostaurin and its metabolites. Negative control: healthy volunteers who received placebo on days 1 to 15 and midostaurin on day 9. Positive control: healthy volunteers who received rifampicin 600 mg once daily on days 1 to 15 and midostaurin on day 9. Midostaurin: patients with advanced systemic mastocytosis who received midostaurin 100 mg twice daily on days 1 to 28.

DMD Fast Forward. Published on November 8, 2017 as DOI: 10.1124/dmd.117.078006
This article has not been copyedited and formatted. The final version may differ from this version.

GM, geometric mean.

Table 1. Input Parameters for Midostaurin, CGP52421, and CGP62221

Parameter	Midostaurin		CGP52421		CGP62221	
	Value	**Reference**	**Value**	**Reference**	**Value**	**Reference**
MW (g/mol)	570.6		586.6		556.6	
logPo:w	5.49	Internal database	4.76	Internal database	4.68	Internal database
pKa	11.2	Predicted[a]	10.8	Predicted[a]	11.2	Predicted[a]
Compound type	Monoprotic base					
f_{up}	0.00015	Internally measured	0.00021	Internally measured	0.00038	Internally measured
B/P	0.55		0.55	Assumed same as parent	0.55	Assumed same as parent
Plasma-binding component	AGP		AGP		AGP	
First-order absorption						
F_a	0.85 (0.65, advSM)	User defined (optimized)				
k_a (h^{-1})	1.5 (0.683, advSM)					
Lag time (h)	0.3					
Q_{gut} (L/h)	5.23	Simcyp predicted				
fu_{gut}	0.3					

Parameter	Midostaurin		CGP52421		CGP62221	
	Value	Reference	Value	Reference	Value	Reference
Peff, man (10^{-4} cm/s)	0.835					
Caco-2 (10^{-6} cm/s)	1.4	Internally measured				
Caco-2 reference (10^{-6} cm/s)	17					
		Minimal with single adjusting compartmental distribution				
Q (L/h)	3 (2.889, AML/advSM)	Estimated from clinical PK data (a single-dose trial)	10	Estimated from clinical PK data (a single-dose trial)	2	Estimated from clinical PK data (a single-dose trial)
Volume (V_{sac} [L/h])	0.82 (0.623, AML/advSM)		1.8		1.1	
V_{ss} (L/h)	1 (0.742, AML/advSM)		1.3		1.3	
Elimination						
Hepatic CL by CYP3A4 (%)	100	Estimated from human ADME study	90	Estimated from human ADME study	90	Estimated from human ADME study
CL_{int}, CYP3A4	9.3	See Elimination				

Parameter	Midostaurin		CGP52421		CGP62221	
	Value	Reference	Value	Reference	Value	Reference
formation of CGP52421 (μL/min/pmol CYP3A4)	(3.9, AML/advSM)					
CL_{int}, CYP3A4	9.3					
formation of CGP62221 (μL/min/pmol CYP3A4)	(3.9, AML/advSM)					
CL_{int}, CYP3A4	6.6		3.18		1.19	
formation of other metabolites (μL/min/pmol CYP3A4)	(2.8, AML/advSM)		(0.557, AML patients)			
Additional HLM clearance (μL/min/mg protein)			48.4 (6.48, AML patients)		18.1	
Active uptake into hepatocytes	1	Default				
CL_R	0	See Elimination				
CYP3A4-related interaction						

Parameter	Midostaurin		CGP52421		CGP62221	
	Value	Reference	Value	Reference	Value	Reference
Reversible inhibition CYP3A4 K_{iu} (μM)	0.25	Internally measured (Supplemental Table 2)	0.44	Internally measured (Supplemental Table 2)	0.25	Internally measured (Supplemental Table 2)
TDI						
K_I, total (μM)	1.02	Internally measured (Supplemental Table 3)	1.97	Internally measured (Supplemental Table 3)	2.01	Internally measured (Supplemental Table 3)
k_{inact} (1/h)	2.8		3.0		4.62	
Induction of CYP3A4 Ind_{max} (fold) $IndC_{50}$ (μM)	9.14 0.0026	Internally measured (Supplemental Table 4) and optimized	10.8 0.0053	Internally measured (Supplemental Table 4) and optimized	11.97 0.0027	Internally measured (Supplemental Table 4) and optimized

[a] Determined using the ADMET Predictor 6.5, Simulations Plus, Lancaster, CA).

ADME, absorption, distribution, metabolism, and excretion; advSM, advanced systemic mastocytosis; AGP, α1-acid glycoprotein; AML, acute myeloid leukemia; B/P, blood-to-plasma ratio; Caco-2, continuous heterogeneous human epithelial colorectal adenocarcinoma cell line; CL, clearance; CL_{int}, intrinsic clearance; CL_R, renal clearance; CYP3A4, cytochrome P450 3A4; $IndC_{50}$, concentration of inducer at half maximal induction; F_a, fraction of dose absorbed; fu_{gut}, fraction of unbound drug in the gut; fu_p, fraction of unbound drug in plasma; HLM, human liver microsome; Ind_{50}, half-maximum induction rate; Ind_{max}, maximal fold induction over vehicle control; k_a, absorption rate constant; K_I, concentration producing a half-maximal rate of activity reduction; k_{inact}, maximal rate of activity reduction; K_{iu}, unbound inhibition constant; logPo:w, water partition coefficient; MW, molecular weight; Peff, man, effective permeability in man; pKa, acid dissociation constant; PK, pharmacokinetics; Q, intercompartmental clearance; Q_{gut}, nominal flow through the gut; V_{sac}, volume of distribution for the single adjustable compartment; V_{ss}, volume of distribution at steady state.

DMD Fast Forward. Published on November 8, 2017 as DOI: 10.1124/dmd.117.078006
This article has not been copyedited and formatted. The final version may differ from this version.

Table 2. Summary of Trial Simulation Design

	Simulated Population	Observed Population	Dosing Regimen	PK Measurement of Substrate
Model performance of midostaurin PK and ketoconazole DDIs	Healthy volunteer	Healthy volunteer	Ketoconazole 400 mg qd on days 1-10 + midostaurin (FMI) 50 mg on day 6	0-120 h, 0-inf
Model performance of midostaurin PK and rifampicin DDIs	Healthy volunteer	Healthy volunteer	Rifampicin 600 mg qd on days 1-14 + midostaurin (FMI) 50 mg on day 9	0-144 h, 0-inf
Model performance of midazolam PK and midostaurin-midazolam DDIs	Healthy volunteer	Healthy volunteer	Midazolam 4 mg qd on days 1 and 6 + midostaurin 100-mg single dose on day 1, 50 mg bid on days 2-4	Day 1: 0-10 h, 0-inf Day 6: 0-10 h

bid, twice daily; DDI, drug-drug interaction; FMI, final market image; inf, infinity; PK, pharmacokinetics; qd, once daily.

DMD Fast Forward. Published on November 8, 2017 as DOI: 10.1124/dmd.117.078006
This article has not been copyedited and formatted. The final version may differ from this version.

Table 3. 4βHC Study Design (CPKC412A2110; registered as EudraCT no. 2009-009895-11)

Population	Study Arm	Treatment	Screening	Study Day													
			Days −14 to −1	Baseline (1)	2	3	4-7	8	9	10	11	12-14	15	16-21	22	23-27	28
Healthy volunteers	Negative control (n = 20)	Placebo qd															
		Midostaurin 50 mg bid															
	Positive control (n = 20)	Rifampicin 600 mg qd															
		Midostaurin 50 mg bid															
	PK assessment	4βHC		*a*					*a*		*a*		*a*				
Patients with advSM	Midostaurin arm (n = 10)	Midostaurin 100 mg bid															
	PK assessment	4βHC		*b*		*b*		*b*					*b*		*b*		*b*

Light-gray highlight indicates receipt of placebo. Medium-gray highlight indicates treatment with rifampicin (a CYP3A4 inducer). Black highlight indicates treatment with midostaurin.

4βHC, 4β-hydroxycholesterol; advSM, advanced systemic mastocytosis; bid, twice daily; PK, pharmacokinetics; qd, once daily.

Blood samples for the assessment of 4βHC in serum were taken as follows:

[a] Healthy volunteers: days 1, 9 (before midostaurin treatment), 11, and 15.

[b] Patients with advSM: days 1, 3, 8, 15, 22, and 28.

DMD Fast Forward. Published on November 8, 2017 as DOI: 10.1124/dmd.117.078006
This article has not been copyedited and formatted. The final version may differ from this version.

Table 4. Summary of Predicted and Observed AUC and C_{max} Ratios With Ketoconazole and Rifampicin

With Co-Administration of Ketoconazole	**Ketoconazole 400 mg qd on Days 1-10 + Midostaurin 50 mg on Day 6**	**AUC_{0-120h} GMR (90% CI range)**		**C_{max} GMR (90% CI range)**	
		Observed	**Predicted**	**Observed**	**Predicted**
	Midostaurin	6.1 (5.0-7.5)	5.8 (5.1-6.5)	1.8 (1.6-2.1)	2.1 (1.9-2.2)
	CGP52421	1.2 (1.0-1.5)	0.6 (0.5-0.7)	0.5 (0.4-0.6)	0.4 (0.4-0.4)
	CGP62221	1.0 (0.8-1.2)	0.6 (0.6-0.7)	0.6 (0.5-0.7)	0.3 (0.3-0.3)
With Co-Administration of Rifampicin	**Rifampicin 600 mg qd on Days 1-14 + Midostaurin 50 mg on Day 9**	**AUC_{0-144h} GMR (90% CI range)**		**C_{max} GMR (90% CI range)**	
		Observed	**Predicted**	**Observed**	**Predicted**
	Midostaurin	0.06 (0.05-0.07)	0.10 (0.09-0.12)	0.27 (0.23-0.31)	0.21 (0.18-0.25)
	CGP52421	0.41 (0.36-0.46)	0.35 (0.31-0.40)	0.65 (0.59-0.72)	0.91 (0.84-0.99)
	CGP62221	0.08 (0.06-0.09)	0.45 (0.40-0.50)	0.63 (0.56-0.70)	1.02 (0.97-1.09)

AUC, area under the curve; C_{max}, maximum concentration; GMR, geometric mean ratio; qd, once daily.

DMD Fast Forward. Published on November 8, 2017 as DOI: 10.1124/dmd.117.078006
This article has not been copyedited and formatted. The final version may differ from this version.

Table 5. Geometric Mean 4βHC Plasma Levels at Each Time Point

	Negative Control (n = 20)	Positive Control (n = 20)	Midostaurin (n = 10; 4 males and 6 females)
GM 4βHC Plasma Levels (CV %) (ng/mL)			
Baseline (day 1)	25.3 (35.5)	22.0 (44.0)	29.2 (43.7)
Day 3	NA	NA	34.1 (43.7)
Day 8	NA	NA	41.7 (39.1)
Day 9	23.4 (36.4)	75.0 (32.1)	NA
Day 11	25.4 (35.9)	89.5 (33.5)	NA
Day 15	23.3 (38.8)	102.7 (27.6)	53.8 (34.7)
Day 22	NA	NA	51.4 (37.1)
Day 28	NA	NA	56.0 (35.6)
GM Percent Change in 4βHC Plasma Levels From Baseline (CV %) (%)			
Day 3	NA	NA	16.8 (0.1)
Day 8	NA	NA	42.9 (−10.3)
Day 9	−7.7 (102)	240.3 (−26.9)	NA
Day 11	0.4 (101)	306.0 (−23.9)	NA
Day 15	−8.1 (109)	366.1 (−37.3)	84.2 (−20.6)
Day 22	NA	NA	76.1 (−14.9)
Day 28	NA	NA	91.7 (18.4)

4βHC, 4β-hydroxycholesterol; CV, coefficient of variation; GM, geometric mean; NA, not applicable.

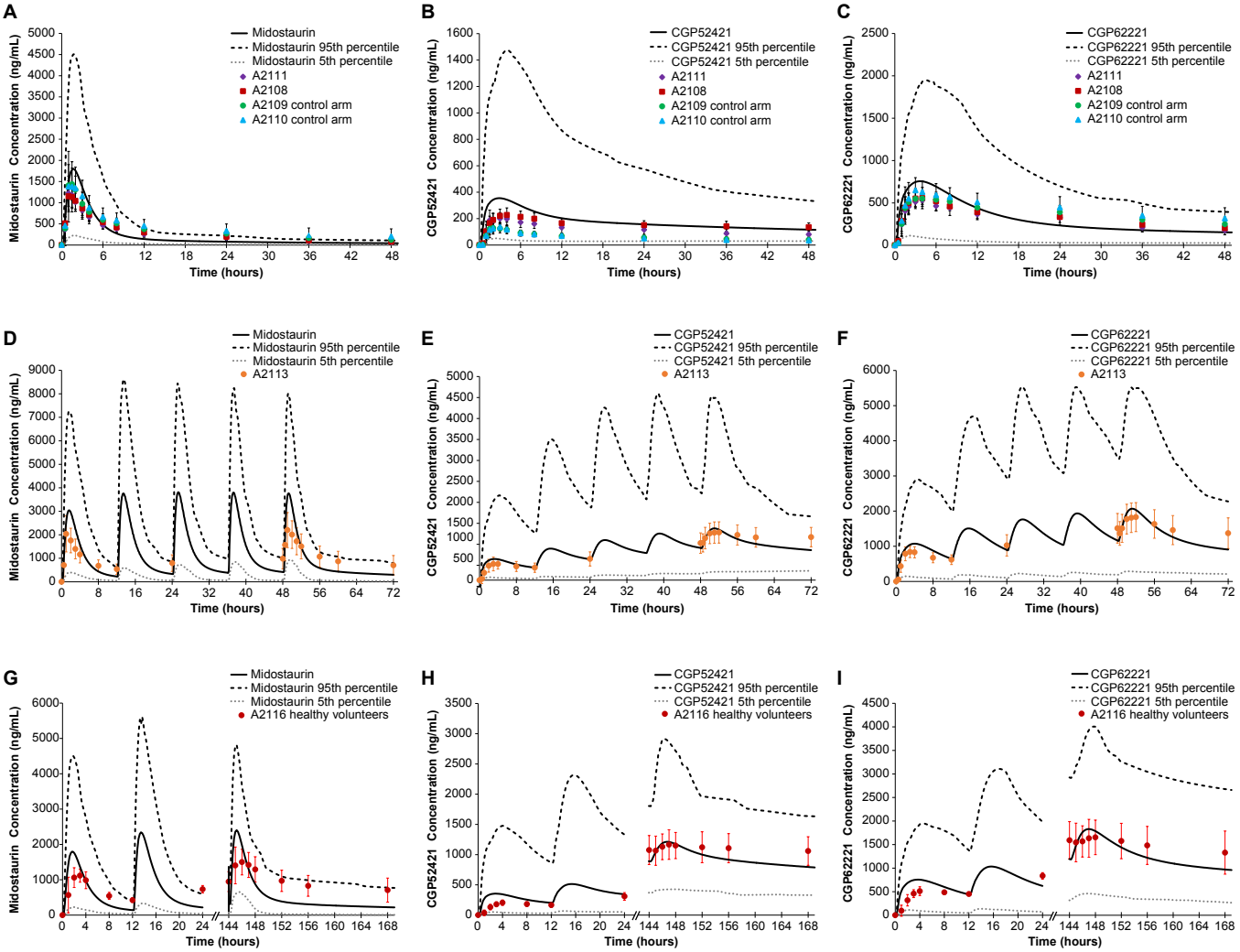
A
Midostaurin Concentration (ng/mL)
Time (hours)
Midostaurin
Midostaurin 95th percentile
Midostaurin 5th percentile
A2111
A2108
A2109 control arm
A2110 control arm
B
CGP52421 Concentration (ng/mL)
Time (hours)
CGP52421
CGP52421 95th percentile
CGP52421 5th percentile
A2111
A2108
A2109 control arm
A2110 control arm
C
CGP62221 Concentration (ng/mL)
Time (hours)
CGP62221
CGP62221 95th percentile
CGP62221 5th percentile
A2111
A2108
A2109 control arm
A2110 control arm
D
Midostaurin Concentration (ng/mL)
Time (hours)
Midostaurin
Midostaurin 95th percentile
Midostaurin 5th percentile
A2113
E
CGP52421 Concentration (ng/mL)
Time (hours)
CGP52421
CGP52421 95th percentile
CGP52421 5th percentile
A2113
F
CGP62221 Concentration (ng/mL)
Time (hours)
CGP62221
CGP62221 95th percentile
CGP62221 5th percentile
A2113
G
Midostaurin Concentration (ng/mL)
Time (hours)
Midostaurin
Midostaurin 95th percentile
Midostaurin 5th percentile
A2116 healthy volunteers
H
CGP52421 Concentration (ng/mL)
Time (hours)
CGP52421
CGP52421 95th percentile
CGP52421 5th percentile
A2116 healthy volunteers
I
CGP62221 Concentration (ng/mL)
Time (hours)
CGP62221
CGP62221 95th percentile
CGP62221 5th percentile
A2116 healthy volunteers

Figure 1

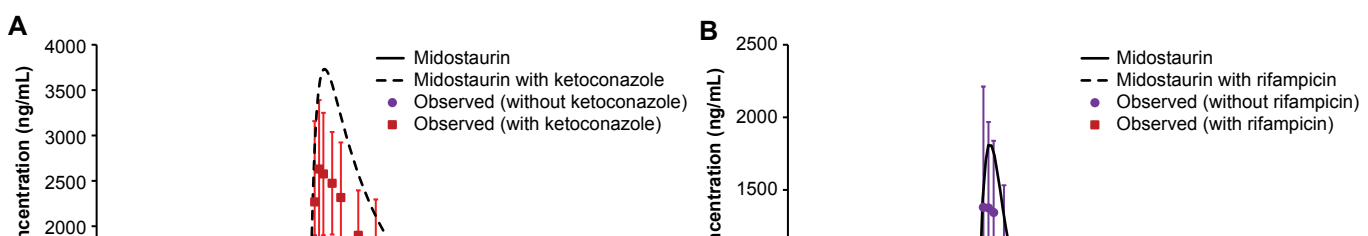
A
Midostaurin Concentration (ng/mL)
4000
3500
3000
2500
2000
1500
1000
500
0
96
108
120
132
144
156
Time (hours)
Midostaurin
Midostaurin with ketoconazole
Observed (without ketoconazole)
Observed (with ketoconazole)
B
Midostaurin Concentration (ng/mL)
2500
2000
1500
1000
500
0
174
186
198
210
222
Time (hours)
Midostaurin
Midostaurin with rifampicin
Observed (without rifampicin)
Observed (with rifampicin)

Figure 2

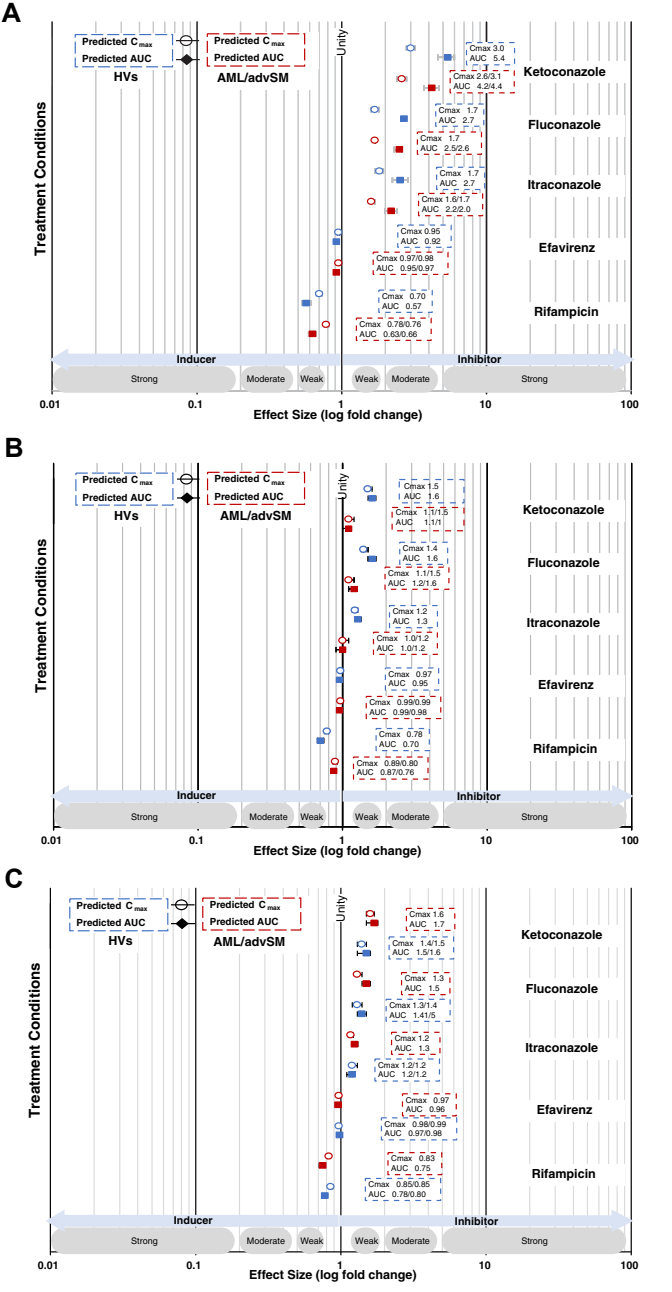
A
Predicted C max
Predicted AUC
HVs
Predicted C max
Predicted AUC
AML/advSM
Unity
Cmax 3.0
AUC 5.4
Cmax 2.6/3.1
AUC 4.2/4.4
Ketoconazole
Cmax 1.7
AUC 2.7
Cmax 1.7
AUC 2.5/2.6
Fluconazole
Cmax 1.7
AUC 2.7
Cmax 1.6/1.7
AUC 2.2/2.0
Itraconazole
Cmax 0.95
AUC 0.92
Cmax 0.97/0.98
AUC 0.95/0.97
Efavirenz
Cmax 0.70
AUC 0.57
Cmax 0.78/0.76
AUC 0.63/0.66
Rifampicin
Treatment Conditions
Inducer
Inhibitor
Strong
Moderate
Weak
Weak
Moderate
Strong
0.01
0.1
1
10
100
Effect Size (log fold change)
B
Predicted C max
Predicted AUC
HVs
Predicted C max
Predicted AUC
AML/advSM
Unity
Cmax 1.5
AUC 1.6
Cmax 1.1/1.5
AUC 1.1/1
Ketoconazole
Cmax 1.4
AUC 1.6
Cmax 1.1/1.5
AUC 1.2/1.6
Fluconazole
Cmax 1.2
AUC 1.3
Cmax 1.0/1.2
AUC 1.0/1.2
Itraconazole
Cmax 0.97
AUC 0.95
Cmax 0.99/0.99
AUC 0.98/0.98
Efavirenz
Cmax 0.78
AUC 0.70
Cmax 0.89/0.80
AUC 0.87/0.76
Rifampicin
Treatment Conditions
Inducer
Inhibitor
Strong
Moderate
Weak
Weak
Moderate
Strong
0.01
0.1
1
10
100
Effect Size (log fold change)
C
Predicted C max
Predicted AUC
HVs
Predicted C max
Predicted AUC
AML/advSM
Unity
Cmax 1.6
AUC 1.7
Cmax 1.4/1.5
AUC 1.5/1.6
Ketoconazole
Cmax 1.3
AUC 1.5
Cmax 1.3/1.4
AUC 1.41/5
Fluconazole
Cmax 1.2
AUC 1.3
Cmax 1.2/1.2
AUC 1.2/1.2
Itraconazole
Cmax 0.97
AUC 0.96
Cmax 0.98/0.99
AUC 0.97/0.98
Efavirenz
Cmax 0.83
AUC 0.75
Cmax 0.85/0.85
AUC 0.78/0.80
Rifampicin
Treatment Conditions
Inducer
Inhibitor
Strong
Moderate
Weak
Weak
Moderate
Strong
0.01
0.1
1
10
100
Effect Size (log fold change)

Figure 3

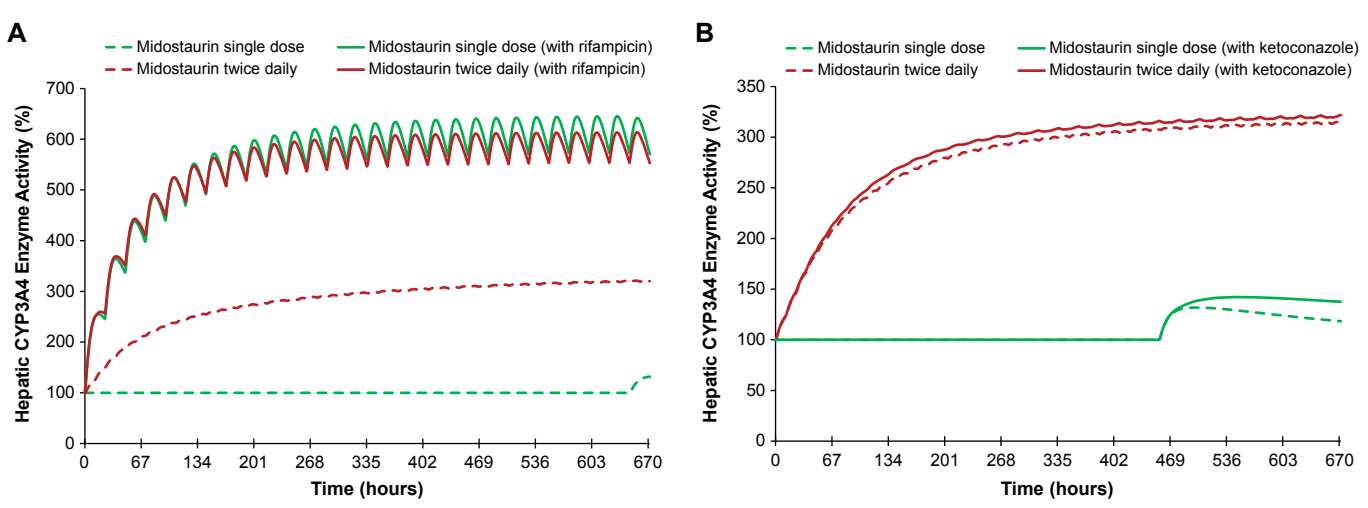
A
Midostaurin single dose
Midostaurin twice daily
Midostaurin single dose (with rifampicin)
Midostaurin twice daily (with rifampicin)
Hepatic CYP3A4 Enzyme Activity (%)
700
600
500
400
300
200
100
0
0
67
134
201
268
335
402
469
536
603
670
Time (hours)
B
Midostaurin single dose
Midostaurin twice daily
Midostaurin single dose (with ketoconazole)
Midostaurin twice daily (with ketoconazole)
Hepatic CYP3A4 Enzyme Activity (%)
350
300
250
200
150
100
50
0
0
67
134
201
268
335
402
469
536
603
670
Time (hours)

Figure 4

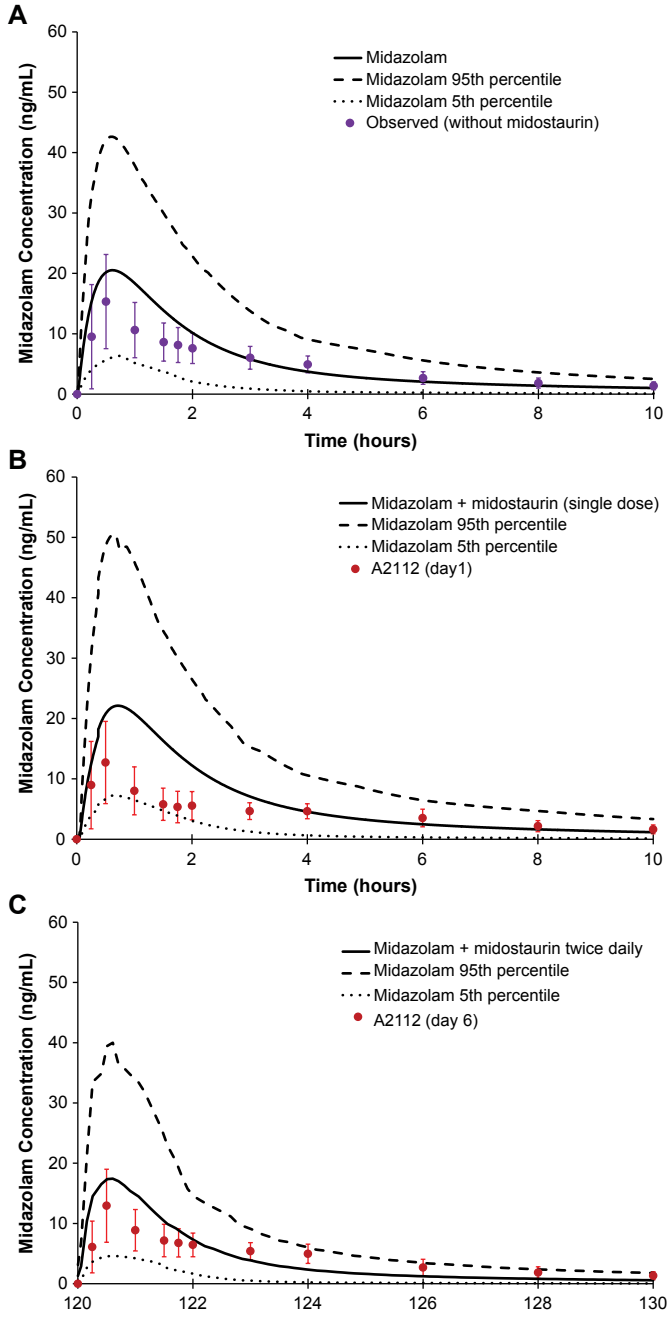
A
Midazolam Concentration (ng/mL)
Midazolam
Midazolam 95th percentile
Midazolam 5th percentile
Observed (without midostaurin)
Time (hours)
B
Midazolam Concentration (ng/mL)
Midazolam + midostaurin (single dose)
Midazolam 95th percentile
Midazolam 5th percentile
A2112 (day1)
Time (hours)
C
Midazolam Concentration (ng/mL)
Midazolam + midostaurin twice daily
Midazolam 95th percentile
Midazolam 5th percentile
A2112 (day 6)
Time (hours)

Figure 5

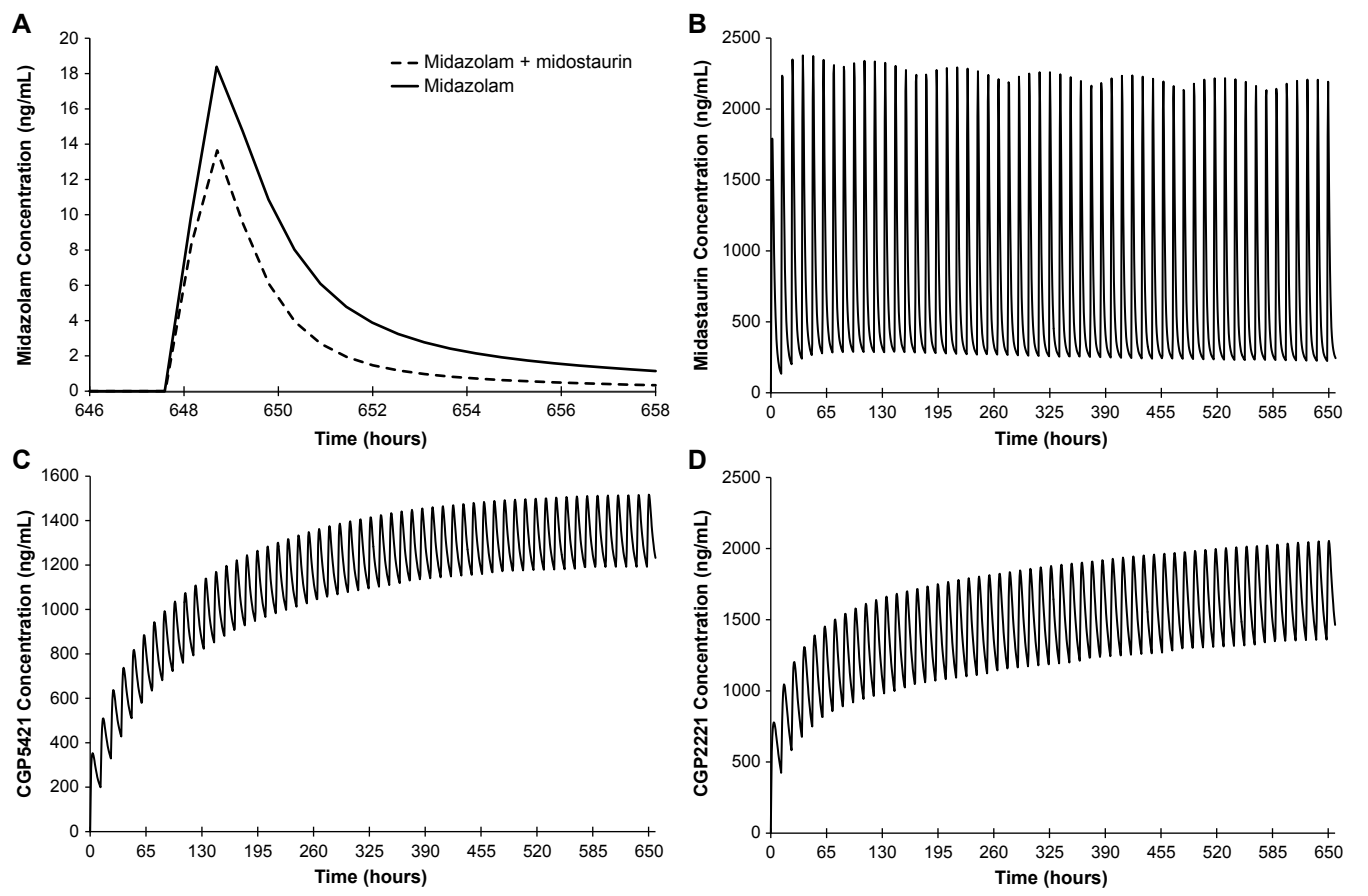
A
Midazolam + midostaurin
Midazolam
Midazolam Concentration (ng/mL)
Time (hours)
B
Midastaurin Concentration (ng/mL)
Time (hours)
C
CGP5421 Concentration (ng/mL)
Time (hours)
D
CGP2221 Concentration (ng/mL)
Time (hours)

Figure 6

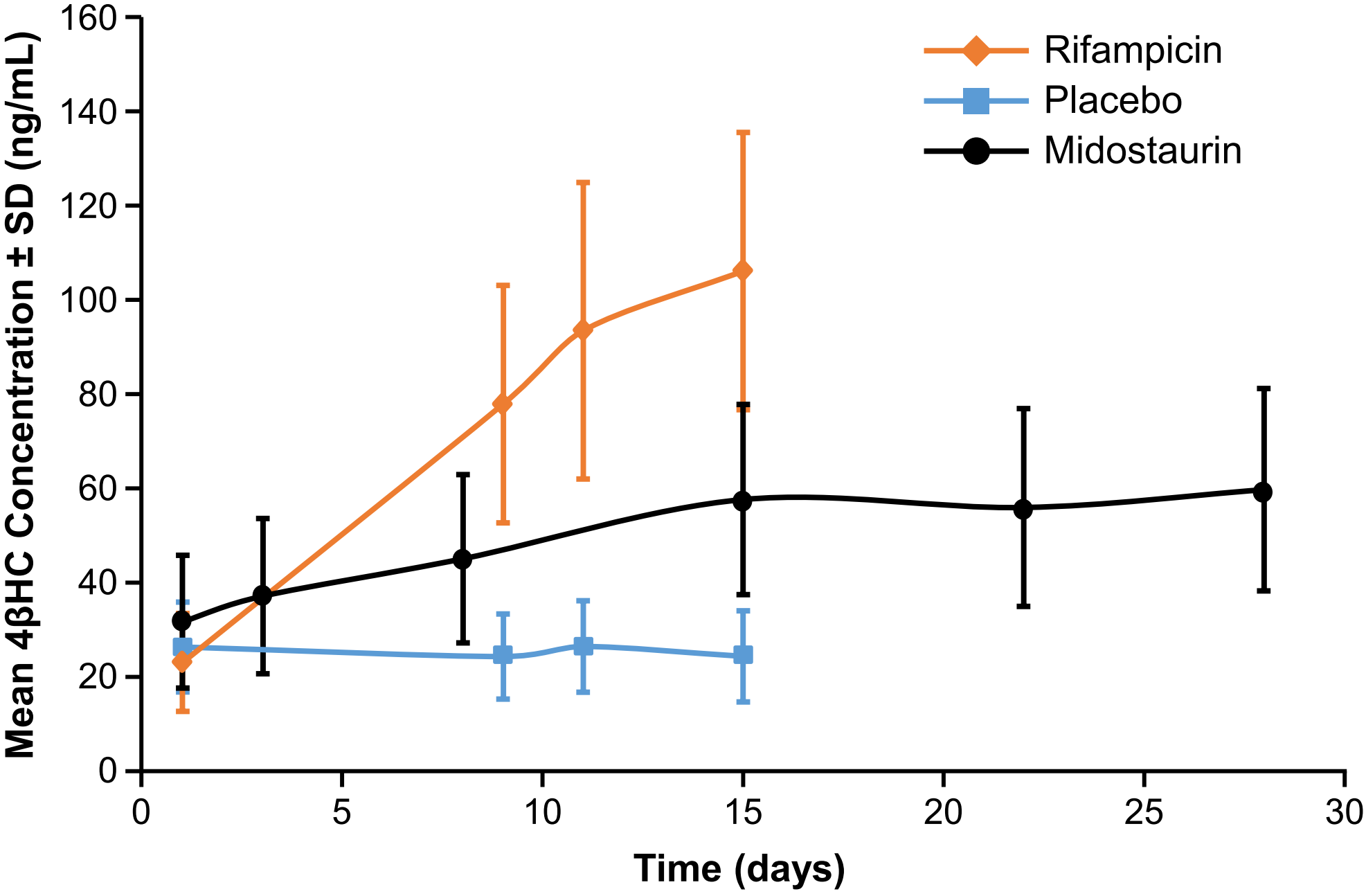

Midostaurin	Time (days)	3	8	15	22	28
	Predicted midazolam GM AUC ratio with midostaurin	0.84	0.60	0.55	0.54	0.54
	Plasma 4βHC GM ratio relative to baseline	1.2	1.4	1.8	1.8	1.9
Rifampicin	**Time (days)**	**9**	**11**	**15**		
	Plasma 4βHC GM ratio relative to baseline	3.2	3.5	4.3		

Figure 7